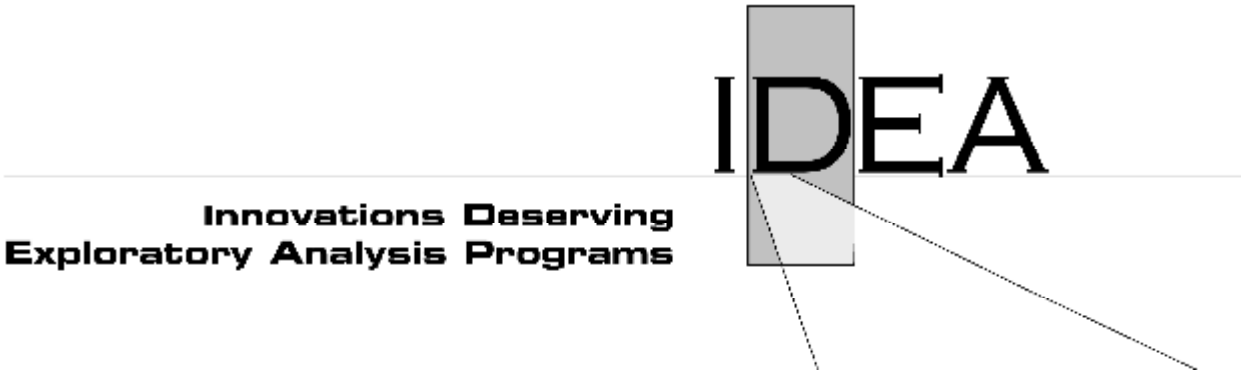

Highway IDEA Program

Rapid, Self-Contained In-Situ Permeameter for Field QA/QC of Pavement Base/Subbase Materials

Final Report for Highway IDEA Project 130

Prepared by:
David J. White, Pavana KR. Vennapusa, Don Eichner, Heath Gieselman, La Zhao, Charles Jahren,
Iowa State University, Ames, IA

August 2010

TRANSPORTATION RESEARCH BOARD
OF THE NATIONAL ACADEMIES

INNOVATIONS DESERVING EXPLORATORY ANALYSIS (IDEA) PROGRAMS MANAGED BY THE TRANSPORTATION RESEARCH BOARD (TRB)

This NCHRP-IDEA investigation was by Research & Technology Corp. completed as part of the National Cooperative Highway Research Program (NCHRP). The NCHRP-IDEA program is one of the three IDEA programs managed by the Transportation Research Board (TRB) to foster innovations in highway and intermodal surface transportation systems. The other two IDEA program areas are TRANSIT-IDEA, which focuses on products and results for transit practice, in support of the Transit Cooperative Research Program (TCRP), and ITS-IDEA, which focuses on products and results for the development and deployment of intelligent transportation systems (ITS), in support of the U.S. Department of Transportation's national ITS program plan. The three IDEA program areas are integrated to achieve the development and testing of nontraditional and innovative concepts, methods, and technologies, including conversion technologies from the defense, aerospace, computer, and communication sectors that are new to highway, transit, intelligent, and intermodal surface transportation systems.

For information on the IDEA Program contact IDEA Program, Transportation Research Board, 500 5th Street, N.W., Washington, D.C. 20001 (phone: 202/334-1461, fax: 202/334-3471, http://www.nationalacademies.org/trb/idea)

RAPID, SELF-CONTAINED IN-SITU PERMEAMETER FOR FIELD QA/QC OF PAVEMENT BASE/SUBBASE MATERIALS

IDEA Program Final Report

NCHRP-130

Prepared for the IDEA Program
Transportation Research Board
The National Academies

Prepared By
David J. White, Ph.D.
Pavana KR. Vennapusa, Ph.D.
Don Eichner
Heath Gieselman
La Zhao
Charles Jahren, Ph.D.

Affiliation
Earthworks Engineering Research Center
Department of Civil, Construction and Environmental Engineering
Iowa State University

December 2009

ACKNOWLEDGMENTS

The National Cooperative Highway Research Program [NCHRP] of the Transportation Research Board [TRB] sponsored this study under the NCHRP Highway Innovations Deserving Exploratory Analysis [IDEA] program. Numerous people assisted the authors in refining research tasks, identifying field projects, and conducting laboratory and field testing. Iowa State University [ISU] Geotechnical Mobile Lab was used for field testing and the Geo-Construction Lab and Spangler Lab were used for laboratory testing.

TABLE OF CONTENTS

EXECUTIVE SUMMARY

Rapid determination of the in-situ hydraulic conductivity for pavement subbase/base layers is critical to ensure that the constructed product meets the design and performance expectations. Currently, no widely accepted specifications or test methods exist for QA/QC of in-situ hydraulic conductivity. This research project produced a ruggedized and repeatable test device known as the Gas Permeameter Test (GPT) for rapid in-situ determination of hydraulic conductivity using an innovative approach based on gas flow measurements through the partially saturated material. The newly developed GPT measures hydraulic conductivity in less than 30 seconds, has a measurement range of about 10^{-4} to 10 cm/s, is completely self contained, and was validated for several different materials. Because rapid measurements can be made in the field, measurements collected in a grid pattern can be used to produce color-coded spatial maps of hydraulic conductivity. Implementation of this device will improve construction process control by identifying and mitigating construction practices that lead to unwanted segregation, and will improve confidence that the assumed design values are achieved, which should contribute to improving the service life of pavements. Figure 1 below highlights the key elements and outcomes from this study: (1) aggregate segregation problem identification, (2) test device conceptual and final design, (3) GPT manufacturing and calibration, and (4) field evaluation of the GPT. Although this research project resulted in a validated and functional device, to fully implement this technology, detailed specifications, field training, and pilot projects are needed.

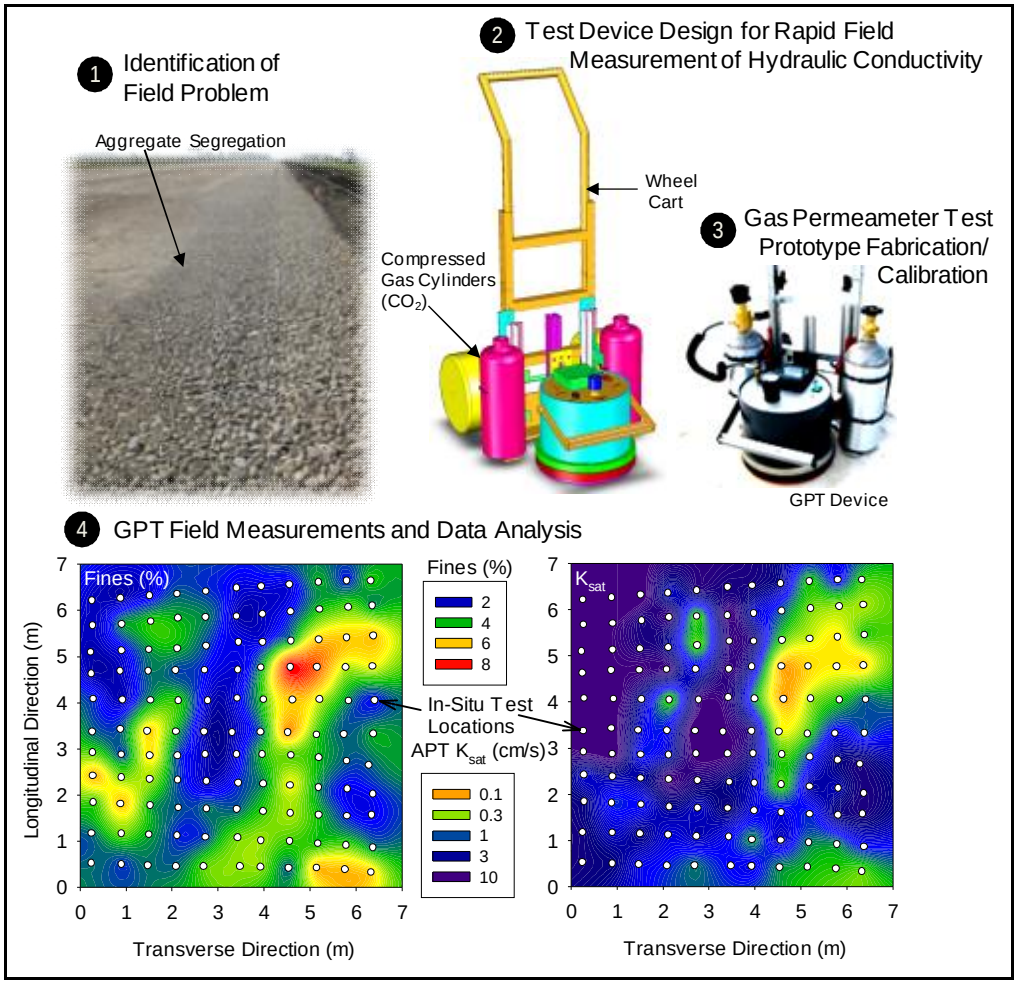

FIGURE 1 Primary steps involved with this study to develop and validate the Gas Permeameter Test device

INTRODUCTION

Drainage in pavement base/subbase layers is critical in achieving the service life of pavements. In practice, most design engineers assume a minimum permeability value in the hydraulic design of permeable base layers based on marginally accurate empirical relationships or limited laboratory testing, but virtually with no field verification. This lack of field measurements provides little confidence in the assumed design values and does not address the fact that permeability is a highly variable parameter. Recent studies have documented that the coefficient of variation [COV] of in-situ permeability is as high as 50% to 400%, making it the most variable engineering parameter in the pavement system. To overcome this problem, a new rapid in-situ permeameter test device that takes less than 30 seconds per test has been designed, manufactured, and validated in this research study. Brief details of the device and its concept, and the research approach to develop and validate the device are described in this report.

IDEA PRODUCT

The product developed from this research study is a new self-contained gas permeameter test [GPT] device for quality control [QC] and quality assurance [QA] testing in-situ to determine saturated hydraulic conductivity of pavement base and subbase layers. Most construction specifications do not address QA/QC testing for permeability of base/subbase layers. The primary reason for this is the lack of a rapid and portable in-situ permeability testing device. Implementing the GPT device as a field QA/QC device will be a significant improvement in the state-of-practice for design and construction of pavement base/subbase layers. By using an in-situ test for permeability that takes less than 30 seconds, multiple tests can be performed in the field allowing for spatial analysis of the results. Spatial maps of the in-situ permeability can be used as QA/QC criteria during base/subbase placement, grading, and compaction to identify field problems such as segregation and particle degradation. Although the focus of the research is for pavement base/subbase materials it is envisioned that this device could also be applied for field QA/QC of pervious pavement materials (i.e., pervious concrete).

CONCEPT OF INNOVATION

This GPT incorporates an innovative design concept that integrates a self-contained pressurized gas system with a self-sealing base plate and a theoretical algorithm to rapidly determine the saturated hydraulic conductivity. The GPT unit weighs about 16 kg and is self-contained with two compressed gas cylinders attached to a wheel cart. More than 50 tests can be performed before refilling the cylinders. The unit can be mounted to the wheel cart on large rubber wheels for easy transporting and handling in the field. The gas flow is controlled using a regulator and a precision orifice. The pressures at the inlet and the outlet of the orifice are monitored using digital pressure transducers and are displayed along with the calculated gas flow rate on a digital display panel. The use of precision orifice for gas flow rate calculations allows for high precision even at low pressures (i.e., < 25 mm of water pressure). The digital display panel is connected to a rechargeable battery mounted inside a ruggedized housing. Test data can be easily transferred to a computer via RS-232 port. More details about the GPT device are provided later.

RESEARCH APPROACH

The research approach included: (a) fabrication of the new device with ruggedized components building on previous experience of the authors'; (b) calibration of flow rate and pressure measurements using a specially fabricated verification panel; (c) extensive laboratory testing on several different granular material types to compare hydraulic conductivity determined from conventional laboratory testing methods with GPT measurements; (d) developing a database of soil-water retention properties (to account for partial saturation) from relationship derived from a literature review; (e) and conducting field investigations at project sites with newly constructed pavement base/subbase layers to evaluate the spatial variability of hydraulic conductivity.

BACKGROUND

Pavement drainage has been recognized in the recent years as a critical component to ensure performance of the pavement layer. Pavement failures are often linked to poor construction and inspection procedures during installation of the pavement drainage components *(1, 2).* According to Cedergren *(2),* the life of a poorly-drained pavement is reduced to one-third or less of the life of a well-drained pavement. Increasingly, new pavements address drainage through the incorporation of a permeable base layer to drain away water entering the pavement system. For hydraulic design of permeable layers, most pavement designers determine the hydraulic conductivity of base materials using empirical relationships with gradation parameters or by conducting a laboratory test *(3, 4, 5).* However, in-situ QA/QC testing as part of the construction is seldom part of the specification. The lack of field QA/QC measurements during construction provide little confidence to the assumed design values and do not address the fact that hydraulic conductivity is a highly variable parameter. The coefficient of variation [COV] for hydraulic conductivity of a given soil is documented to be on the order of 50% to 400% *(6, 7, 8).* Some of the factors that contribute to this high level of variability include: (1) segregation caused during construction; (2) particle breakdown from compaction and construction traffic; and (3) inherent variations in the material gradation and morphology *(8).*

Various in-situ permeability testing methods developed over the last five decades for agricultural, petroleum, landfill, and pavement surface, and pavement base/subbase layer applications are summarized in Table 1. Water, air, nitrogen, and vacuum have been used as permeating fluids to determine permeability. Obstacles for widespread use of most of these devices, especially of the tests conducted using water, have included difficulty in conducting the tests (i.e., sealing, transporting water, fines migration, trapped air bubbles, etc.), lengthy testing time, verification of test measurements, and clearly showing the benefit for QC/QA. As an improvement over these techniques, a prototype air permeameter test device was developed at Iowa State University to rapidly determine saturated hydraulic conductivity (K_{sat}) in-situ for pavement base/subbase materials *(8).*

TABLE 1 Summary of various in-situ permeability testing equipment

Application	Device *(Reference)*	Permeant
Agricultural/Forest soils	Air Permeameters *(9, 10, 11, 12, 13)*	Air
	Light Weight Air Mini Permeameter *(14)*	Air
Rocks (Petroleum Industry)	Mini Permeameter *(15)*	Air
	Air Probe Mini Permeameter *(16)*	Air
Desert soils	Soil Corer Air Permeameter *(17)*	Air
Soils (applicable for $K_{sat} < 10^{-8}$ cm/s)	Air Entry Permeameter *(18)*	Water
Soils (applicable for $K_{sat} = 10^{-2}$ to 10^{-6} cm/s)	Single Ring Infiltrometer *(19)*	Water
	Double Ring Infiltrometer *(20)*	Water
Soils (applicable for $K_{sat} < 10^{-6}$ cm/s)	Double Tube Test Method *(21)*	Water
	Borehole Permeameter Methods (*22,23)*	Water
Dry Granular Soils	Gas Flow Permeability Device *(24)*	Nitrogen
HMA layers and dense aggregate layers	NCAT Field Permeameter *(25)*	Water
	Air Induced Permeameter *(25)*	Air/Vacuum
PCC/Asphalt surface	Dynamic Air Outflow Meter *(26)*	Air
	Dynamic Permeability Testing Device *(27)*	Water
	Static Water Permeability Device *(27)*	Water
	Static Water Outflow Meter *(28)*	Water
	Static Air Permeability Meter *(27,29)*	Air
Aggregate base/subbase	Field Permeability Testing Device *(30)*	Water
Aggregate base/subbase	Field Permeameter *(31)*	Water
Aggregate base/subbase	Air Permeameter Test Device *(8)*	Air

The prototype air permeameter test device weighed about 18 kg (40 lb), and consisted of a contact ring, console, two flow meters, and two differential pressure gauges. The pressure gauges were attached to the outflow end of the contact ring. A compressed gas source with regulator was connected to the device through a flexible hose. Closed-cell medium density neoprene foam was attached to the bottom of the contact ring to prevent leakage between the bottom of the contact ring and the ground surface. The durometer and thickness of the foam were adjusted to site-specific conditions to provide the necessary seal. A theoretical derivation was developed to estimate K_{sat} from the device air pressure and flow rate measurements *(32).* The prototype device was tested in the field to verify the theoretical derivation and compare with laboratory measurements obtained using a specially fabricated 300 mm diameter by 300 mm high large scale aggregate compaction mold laboratory permeameter [LSLP].

The prototype device was also used to investigate spatial variability of pavement base/subbase layer K_{sat} and the change in K_{sat} as a function of percent fines content (passing #200 sieve) in the field *(8, 33).* Field tests were conducted on final compacted base/subbase layers in a square grid pattern at 25 to 30 locations over an area of about 60 to 100 m^2. Bag samples of base material were obtained to determine the fines content. In the field, it was quickly determined that a significant advantage of this device was the speed at which tests could be performed (< 1 minute per test). This was considered a major improvement over previous in-situ permeability testing devices in that many measurements could be made over a small area allowing examination of spatial variability.

Although the prototype was simple, relatively portable, and provided rapid in-situ measurements, significant improvements to this device were needed to improve ease in handling the instrument and obtaining more accurate air flow rate and pressure readings. The following chapter provides detailed information on the design of the new GPT prototype device and its components.

GPT DEVELOPMENT AND COMPONENTS

Three-dimensional [3D] design drawings of the new GPT device and its components are shown in Figure 2. Additional cross-sectional drawings of the GPT are provided in Appendix A. Pictures of the GPT device and components, the case for shipping and handling, and the wheel cart are shown in Figure 3. The GPT unit weighs about 16 kg (35 lbs) and is self-contained with two compressed gas cylinders attached to the wheel cart. With two carbon dioxide (CO_2) cylinders, more than 50 tests can be performed before refilling the cylinders. The unit can be mounted on to the wheel cart on large rubber wheels to allow for easy transporting and handling in the field. Gas flow is controlled using a regulator (TesCom model 44-2213-242) and a replaceable precision orifice (manufactured by Lenox Laser). The gauge pressure at the inlet and the outlet of the orifice are monitored using digital pressure transducers (manufactured by Dwyer) to calculate flow rate (calculation details are provided in the following section). The use of a precision orifice to calculate flow rate allows for high precision even at low pressures (i.e., < 25 mm of water pressure). The inlet pressure transducer measurement range is 0 to 1724 kPa (0-250 psi), and the outlet pressure transducer measurement range is 0 to 76 (0-3 in) mm of water [H_20]. The inlet and outlet gauge pressures and calculated flow rate measurements are displayed on a programmable digital display panel (OTEK model HI-Q126 triple digit display) attached to the top cover plate. The digital display panel is connected to a rechargeable battery mounted inside the ruggedized housing. Data obtained during the test can be transferred to a computer via the RS-232 port and the auxiliary switch on the top cover plate. The base plate is fabricated using an abrasive resistant polymer and is replaceable if needed. A polyurethane base seal is attached to the base plate. The test is performed by placing the GPT unit on closed-cell compressible foam (not shown in Figure 2) to effectively seal the base and prevent gas leakage. The effectiveness of the seal is discussed later in this chapter.

Four different orifice sizes were used in this research study for testing a wide range of materials. Each orifice represents a fixed range of flow-pressure conditions and therefore a limited range of hydraulic conductivity values. Discussion on flow rate calculation using precision orifice pressure measurements, pressure transducer and flow rate calibration, and base seal inspection are provided in the following sections. The following terminology is used in presenting the results with different orifice sizes:

- GPT(A) – orifice diameter = 2982.00 μm
- GPT(B) – orifice diameter = 870.95 μm
- GPT(C) – orifice diameter = 293.66 μm
- GPT(D) – orifice diameter = 149.41 μm

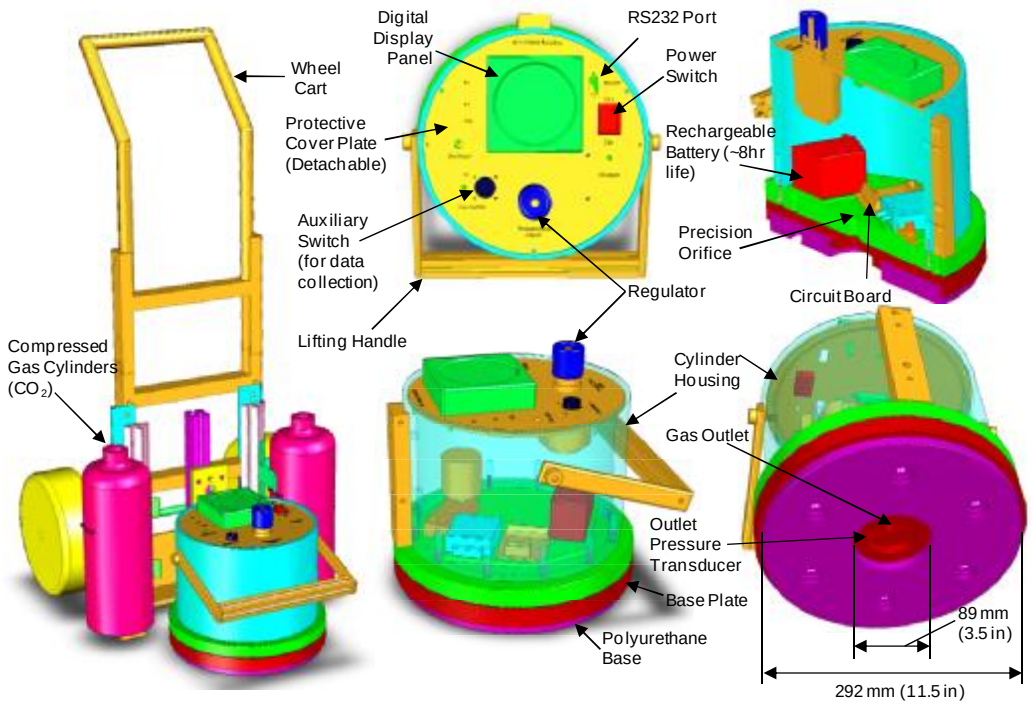

FIGURE 2 Three-dimensional sketch of the GPT device and components

FIGURE 3 Internal ruggedized sensor components, regulator, and circuit board for digital display (left); pelican case for shipping and handling (middle); wheel cart pick-up device with two aluminum CO_2 cans (right)

FLOW RATE CALCULATION FROM PRESSURE MEASUREMENTS

The pressures at the inlet and outlet of the orifice are used to calculate the flow rate using the following equation *(34)*:

$$Q = \frac{0.01749}{60} \times \frac{P_{i(a)}}{29.7} \times \sqrt{\frac{29}{M}} \times CF \times \sqrt{\frac{528}{T}} \times d^2 \qquad (1)$$

where: Q = volumetric flow rate (cm^3/s); $P_{i(a)}$ = absolute pressure at the orifice inlet (psi); M = molecular weight of gas (Air = 29, Nitrogen = 28, CO_2 = 44); T = temperature (Rankine); CF = correction factor based on $\Delta P/P_i$ (see Appendix B); $\Delta P = P_{i(a)} - P_{o(a)}$; $P_{o(a)}$ = absolute pressure at the orifice outlet (psi); d = orifice diameter (µm).

Of all the parameters in equation 1, the flow rate calculation is primarily affected by the change in $P_{i(a)}$, d, M, and CF. Temperature has minimal effect in the flow rate calculation, i.e., < 5% over a change in temperature change from 0 °C (32°F) to 40°C (110°F). To avoid difficulties in programming the digital meter using multiple parameters in equation 1, a three-parameter hyperbolic model was fit to the pressure-flow relationship as shown in Figure 4. A constant temperature of 20°C was assumed for the model. Hyperbolic model parameters for air, CO_2, and nitrogen have been developed for the four different orifice sizes used in this study. The model parameters and the program code are provided in Appendix B.

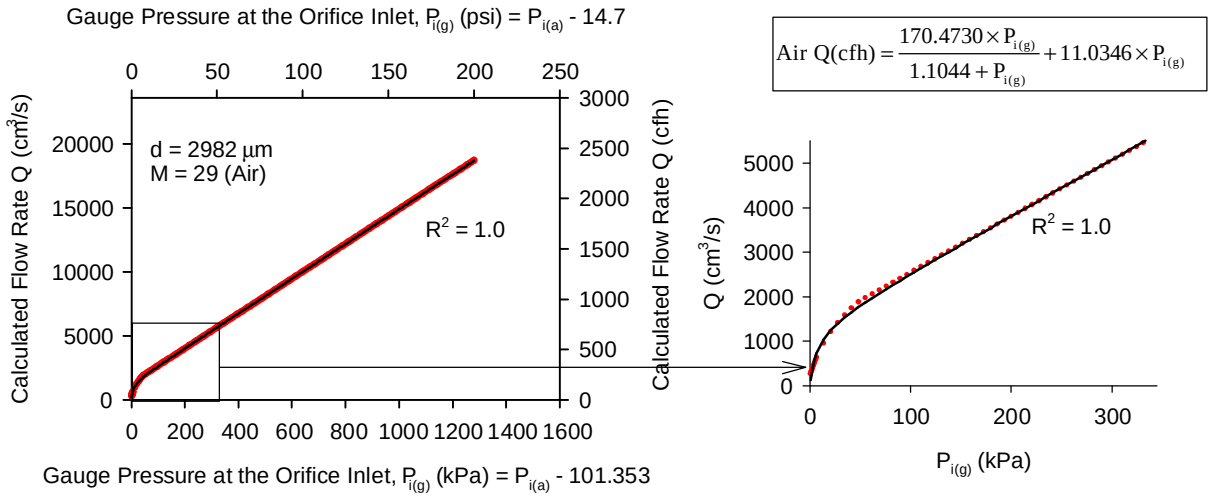

FIGURE 4 Pressure flow relationship (for air) using a three parameter hyperbolic model

PRESSURE TRANSDUCER AND FLOWRATE CALIBRATION

A verification panel was specially fabricated for inspection of the GPT unit and calibration of the components (see Figure 5). The panel consists of two high resolution differential pressure gauges and a digital flow meter. The digital pressure transducers measuring the $P_{i(g)}$ and $P_{o(g)}$ were tested and calibrated with pneumatic pressure signals to verify zero and span settings using an Altek 134-2 milliamp calibrator. Pressure was applied with a precision regulator and monitored with high resolution water column manometers (0 to 25.4 mm of H_20 range) and a mechanical gauge (0 to 12.5 mm of H_20 range). During the test, current at the "zero" input level and "full scale" when maximum input pressure was applied were measured as 4 and 20 milliamps, respectively. The digital display meter was also calibrated using an Altek 134-2 milliamp calibrator. The flow rate calculated using the procedure described above was compared with measurements from a digital flow meter over a $P_{i(g)}$ range of 0 to 345 kPa (0 to 50 psi). The comparison test results are presented in Figure 5 which shows excellent agreement between the measured and calculated flow rate values.

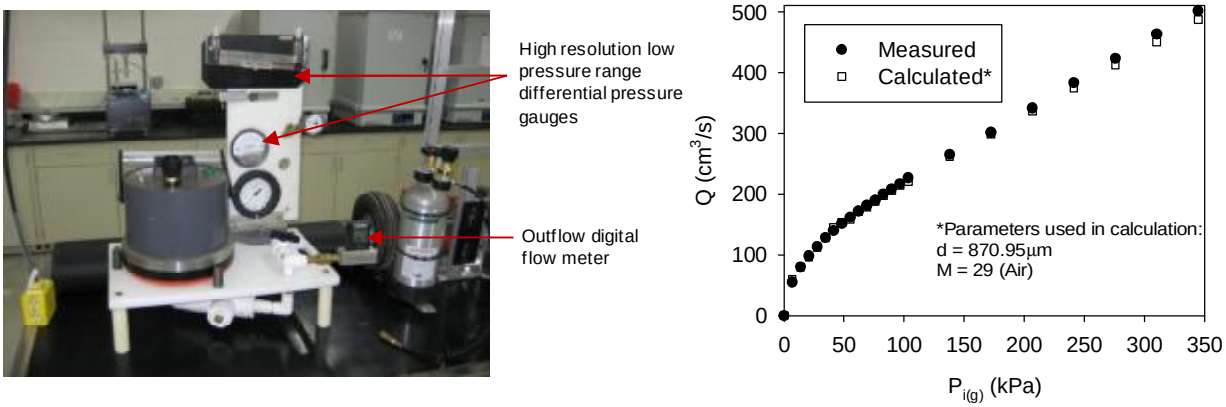

FIGURE 5 GPT pressure and flow sensor verification panel (left) and measured versus calculated flow rate (right)

BASE SEAL INSPECTION

Epoxy disks with rough surfaces were specially made to investigate the effectiveness of the base seal (Figure 6). One disk was made of pea gravel (100% passing 9.5 mm sieve) and the other was made of crushed limestone (100% passing 25.4 mm sieve). Both discs represented very rough conditions for the respective materials to simulate field conditions. The test procedure involved placing the GPT unit on several different soft compressible foam materials placed on the aggregate epoxy discs and monitoring the pressure buildup at the orifice outlet ($P_{o(g)}$) with no gas flow. These base seal verification tests can be performed periodically as a quality control measure. After testing several different materials, slow recovery foam with firmness in the range of 1 to 2 was verified to provide an excellent seal with no leakage, even on the very rough conditions of the aggregate-epoxy discs. Although the seal was verified, it was observed that the foam material can become worn over time and therefore is recommended that the seal be replaced periodically (about every 50 tests). The seals were cut to exact dimensions using a water jet cutting system. The cost for a replacement seal is about $25.

FIGURE 6 GPT device polyurethane base (left) and foam seal (middle and right) (middle and right photos show the device seated on epoxy aggregate disks made with crushed lime stone for checking the base seal)

SATURATED HYDRAULIC CONDUCTIVITY CALCULATIONS

Derivation of a relationship to calculate the saturated hydraulic conductivity from the gas flow and pressure measurements is possible with an expansion of Darcy's Law considering compressibility of gas, viscosity of gas, and gas flow under partially saturated conditions. Details of the derivation are presented in White et al. *(32)*. In brief, to develop this relationship first an equation to estimate gas permeability is derived (equation 2) and then the effect of partial saturation is taken into account to determine relative gas permeability (K_{rg}), which is then converted to water saturated hydraulic conductivity (K_{sat}) (equations 3 to 5). An approach presented by Brooks and Corey *(35)* is used to determine the K_{rg}.

$$K_{gas} = \left[\frac{2\mu_{gas} Q P_1}{r G_o \left(P_1^{\,2} - P_2^{\,2} \right)} \right] \tag{2}$$

$$K_{sat} = K_{gas} \times \frac{\rho g}{\mu_{water} K_{rg}} \tag{3}$$

$$K_{rg} = (1 - S_e)^2 \left(1 - S_e^{((2+\lambda)/\lambda)} \right) \tag{4}$$

$$\Rightarrow K_{sat} = \left[\frac{2\mu_{gas} Q P_1}{r G_o \left(P_1^{\,2} - P_2^{\,2} \right)} \right] \times \frac{\rho g}{\mu_{water} (1 - S_e)^2 \left(1 - S_e^{((2+\lambda)/\lambda)} \right)} \tag{5}$$

where: K_{sat} = saturated hydraulic conductivity (cm/s); K_{gas} = gas permeability; K_{rg} = relative permeability to gas; μ_{gas} = kinematic viscosity of the gas (PaS); Q = volumetric flow rate (cm^3/s); P_1 = absolute gas pressure on the soil surface (Pa) $P_{o(g)}$ x 9.81 + 101325; $P_{o(g)}$ = gauge pressure at the orifice outlet (mm of H_20); P_2 = atmospheric pressure (Pa); r = radius at the outlet (4.45 cm); G_o= Geometric factor (dimensionless factor see Figure 7), S_e = effective water saturation [$S_e = (S - S_r)/(1-S_r)$]; λ = Brooks-Corey pore size distribution index; S_r = residual water saturation; S = water saturation; ρ = density of water (g/sm^3); g = acceleration due to gravity (cm/s^2); μ_{water} = absolute viscosity of water (gm/cm-s). The geometric factor (G_o) was developed for steady state gas flow considering the GPT device geometry, sample geometry, and three dimensional flow conditions using an approach proposed by Goggin et al. *(16)*.

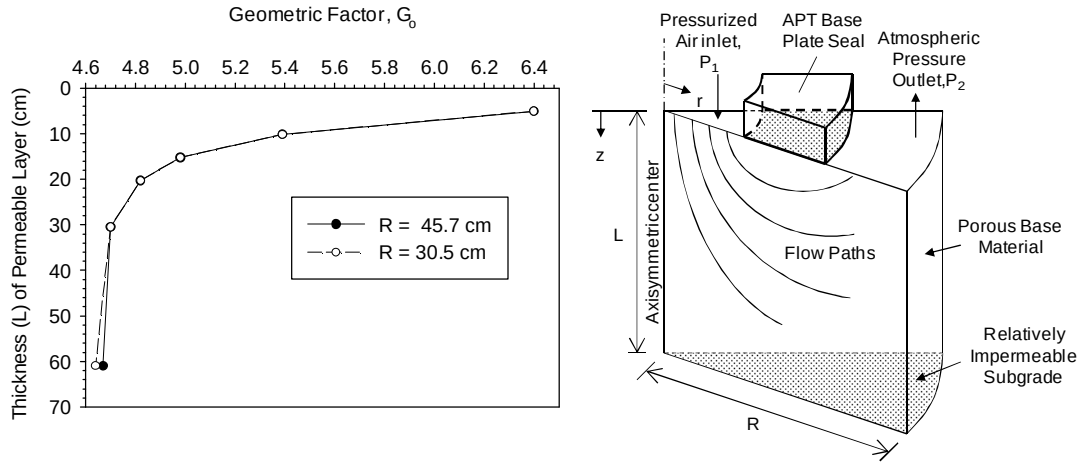

FIGURE 7 Graph to determine the geometric factor G_o for K_{sat} calculation

The degree of saturation (S) values can be obtained from in-situ dry unit weight and moisture content measurements. The S_r and λ parameters can be obtained by determining the soil-water retention properties (also known as soil water characteristic curves [SWCC]) of the materials. Previous work with the prototype air permeability test device *(32)* involved selection of these parameters based on appropriate material type from the literature. According to Brooks and Corey *(35)*, λ is generally smaller for materials having a wide range of pore sizes and larger for materials having relatively uniform pore sizes. Cote and Konrad *(36)* report that S_r is close to zero for aggregate base course materials

with mainly coarse particles. Levorson *(37)* indicates that the S_r for granular soils is generally close to the "bulking" moisture content. Bulking moisture contents for granular base materials are generally in the range of about 3 to 5 percent based on dry weight.

Tests to determine the SWCC parameters can be time-consuming and require precise calibration of test equipment. As an alternative, empirical relationships from material gradation properties are used in the mechanistic-empirical pavement design guide [MEPDG] *(38).* A modified version of the Fredlund and Xing *(39)* SWCC model shown in equation 6 is used in the MEDPG Enhanced Integrated Climatic Model [EICM]. This approach was adopted for determination of the GPT input values. For the materials used in this study, SWCC parameters were derived and then S_r and λ values were calculated using the Brooks and Corey *(*35*)* approach.

$$\theta_w = C(h) \times \left[\frac{\theta_{sat}}{\left[\ln\left[2.7183 + \left(\frac{\psi}{a_f} \right)^{b_f} \right] \right]^{c_f}} \right] \tag{6}$$

$$\text{with } C(h) = \left[1 - \frac{\ln\left(1 + \frac{\psi}{\psi_r} \right)}{\ln\left(1 + \frac{1.45 \times 10^5}{\psi_r} \right)} \right] \tag{7}$$

where: ψ = matric suction (psi), θ_w = volumetric moisture content (%), a_f, b_f, c_f, and ψ_r = SWCC curve fitting parameters correlated with material gradation properties using a database of 154 non-plastic granular materials *(38)* as shown in the equations below.

$$a_f = 1.14 a_i - 0.5 \text{ (Note: when } a_f \text{ results in negative value, use } a_f = 1.0) \tag{8}$$

$$a_i = -2.79 - 14.1 \log(D_{20}) - 1.9 \times 10^{-6} P_{200}^{4.34} + 7 \log(D_{30}) + 0.055 D_{100} \tag{9}$$

$$D_{100} = 10^{\left[\frac{40}{m_1} + \log(D_{60}) \right]} \tag{10}$$

$$m_1 = \frac{30}{\left[\log(D_{90}) - \log(D_{60}) \right]} \tag{11}$$

$$b_f = 0.936 b - 3.8 \tag{12}$$

$$b = \left(5.39 - 0.29 \ln\left[P_{200} \left(\frac{D_{90}}{D_{10}} \right) \right] + 3 D_0^{0.57} + 0.021 P_{200}^{1.19} \right) \times m_1^{0.1} \tag{13}$$

$$D_0 = 10^{\left[\frac{-30}{m_2} + \log(D_{30}) \right]} \tag{14}$$

$$m_2 = \frac{20}{\left[\log(D_{30}) - \log(D_{10}) \right]} \tag{15}$$

$$c_f = 0.26 e^{0.785 \times c} + 1.4 D_{10} \tag{16}$$

$$c = \log\left(m_2^{1.15} \right) - \left(1 - \frac{1}{b_f} \right) \tag{17}$$

$$h_r = 100 \quad (18)$$

where: D_{10} = grain size corresponding to 10% passing by weight (mm); D_{20} = grain size corresponding to 20% passing by weight (mm); D_{30} = grain size corresponding to 30% passing by weight (mm); D_{60} = grain size corresponding to 60% passing by weight (mm); D_{90} = grain size corresponding to 90% passing by weight (mm); P_{200} = percentage material passing the #200 sieve (%).

For reference, typical S_r and λ values reported in the literature and values calculated based on material gradation parameters using the above described approach (grouped into soil classification for convenience) are summarized in Table 2. Typical field saturation values reported for granular base/subbase materials in the literature are summarized in Table 3.

TABLE 2 Summary of residual saturation and pore size distribution index values reported in the literature and typical values calculated using equations 6 to 18 for granular materials

Material Type or USCS Classification	Residual Saturation (S_r)	Pore Size Distribution Index, λ	Reference
Touchet Silt Loam	18 to 22	1.02 to 1.70	*(43)*
Columbia Sandy Loam	18 to 22	1.27 to 1.70	
Unconsolidated Sand	8 to 9	4.02 to 4.75	
Volcanic sand	16	2.29	*(35)*
Fine sand	17	3.7	
Glass beads	9	7.3	
Natural Sand Deposits	—	4	*(44)*
Crushed Granite	—	0.33 to 0.36	*(36)*
Crushed Shale	—	0.23 to 0.27	
Crushed Limestone	—	0.22 to 0.31	
Range of values for typical filter materials and open graded bases *(45)*			Calculated using equations 6 to 18
SW (Filter Materials)	10 to 11	0.65 to 2.15	
SP (Filter Materials)	10	11.15	
GP (Open Graded Bases)	1 to 2	17.26 to 18.20	
Range of values determined for granular materials used in this study			Calculated using equations 6 to 18
SP	10	2.20 to 4.08	
SW-SM	11	0.54	
GP	2 to 5	3.65 to 4.62	
GP-GM	11 to 15	0.59 to 0.98	

TABLE 3 Summary of measured field saturation values reported in the literature for granular base/subbase materials

Material Type	Classification (USCS, AASHTO)	Field Saturation, S (%)†		Reference
		Mean	COV (%)	
Crushed Lime Stone	GP-GM, A-1-a	16	20	*(32)*
Reclaimed Asphalt	GP-GM, A-1-a	28	49	
Crushed Recycled Concrete	GW-GM, A-1-a	45	9	
Crushed Lime Stone	GP-GC, A-1-a	19	17	
Crushed Recycled Concrete	GP, A-1-a	37	19	
Crushed Gravel	SP-SM, A-1-b	53	9	*(46)*
Crushed Gravel	SP-SM, A-1-b	44	31	
Flex Base Material	GP-GM, A-1-a	58	15	*(47)*
Crushed Sandstone	GW	62	9	*(48)*
Crushed Limestone	GP-GM, A-1-a	36	19	*this project*
Crushed Slag	GP-GM, A-1-a	24	24	*this project*
Cement Treated Base	GP, A-1-a	35	15	*this project*

†field saturation values determined from in-situ moisture and dry unit weight measurements using a nuclear gauge.

A parametric study was conducted to assess the sensitivity of the various parameter values (S, S_r, λ, G_o, $P_{o(g)}$ and Q) in equation 5 to evaluate the overall significance of a given parameter value on the calculated saturated hydraulic conductivity. Results of that parametric study are presented in Figure 8. Comparatively, $P_{o(g)}$, Q, and S values have the maximum influence and S_r, λ, and G_o have minimum influence on the calculated K_{sat} value. Following are some key points on the influence S_r, λ, and G_o:

- For the range of λ summarized in Table 2 (0.5 to 18.2), the calculated K_{sat} increases with increasing in λ by about 1.1 to 2.2 times for an increase in S from 20 to 80%. There is negligible influence of λ on K_{sat} for S < 20%.
- Based on values summarized in Tables 2 and 3, the typical range of S_r = 0 to 20% and S = 0 to 70% for granular materials. For the range of S = 0 to 70%, the calculated K_{sat} decreases by about 1.8 times or less with increase in S_r from 0 to 20%.
- The G_o value varies with the thickness of the sample. For an increase in sample thickness from 5 cm to 61 cm, the calculated K_{sat} increases by about 1.4 times. G_o values should be selected based on field thickness measurements.

$P_{o(g)}$ and Q values are measured by the GPT device and as noted earlier, determination of S will require in-situ moisture content and dry unit weight tests. Selection of the S_r and λ from literature (e.g., Table 2) or based on gradation parameters (as described above) will be sufficient for obtaining meaningful comparable K_{sat} measurements in-situ.

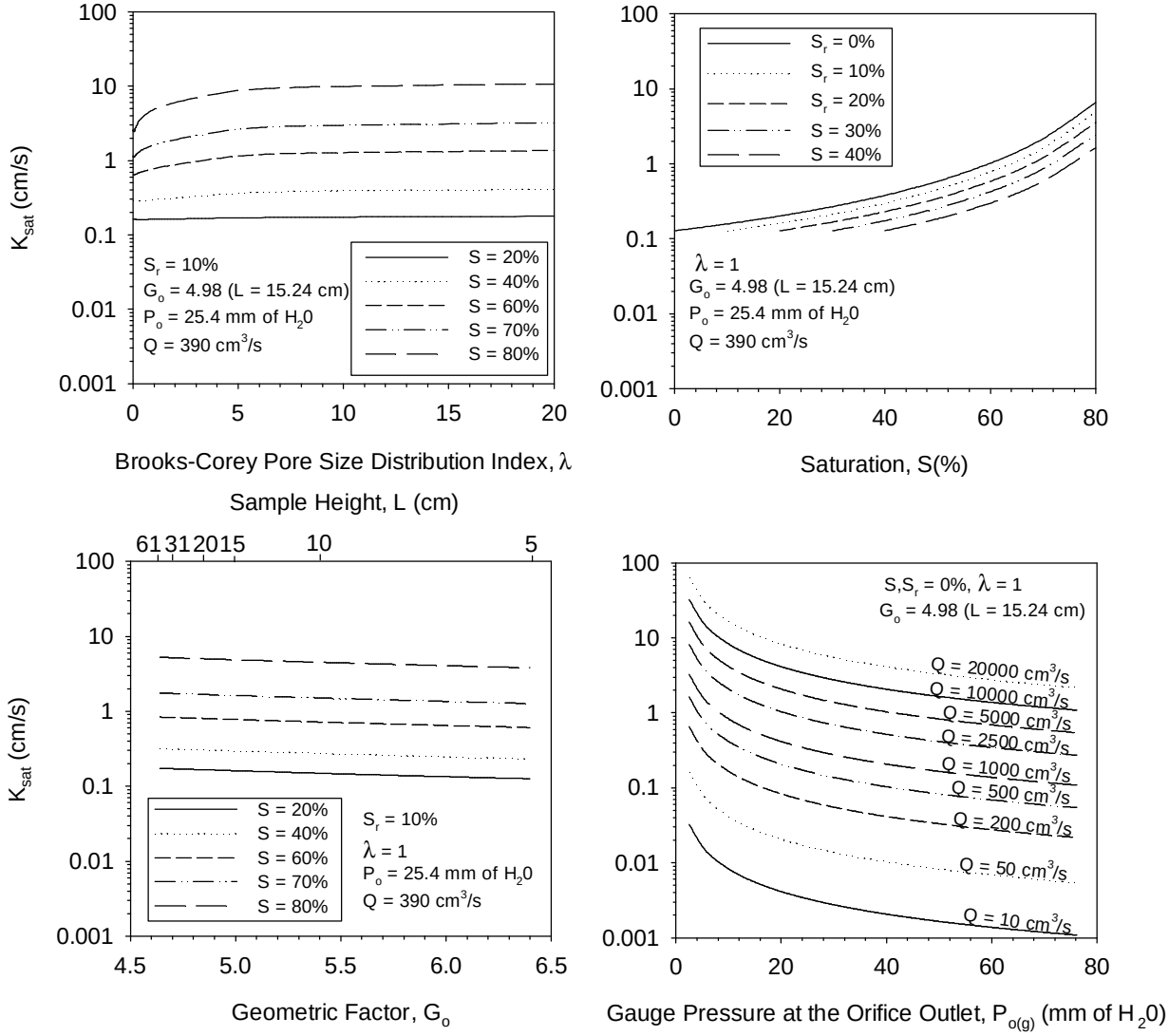

FIGURE 8 Influence of λ, S, S_r, G_o, P_o, and Q in K_{sat} calculation

LAB VERIFICATION AND REPEATABILITY

This chapter presents laboratory testing performed on materials to determine material index properties (i.e., gradation, classification, soil-water retention properties, etc.), obtain comparison hydraulic conductivity test measurements using water and the GPT device, evaluate GPT repeatability, and evaluate the effects of partial saturation on the calculated K_{sat}. A stand-alone standard test protocol, calculations, and periodic laboratory verification and inspection guidelines were developed and are included in Appendix C.

MATERIAL GRADATION AND SOIL WATER RETENTION PROPERTIES

The materials used as part of this research study are summarized in Table 4. A summary of material index properties including gradation parameters, classification (according to American Association of State Highway and Transportation Officials [AASHTO] and Unified Soil Classification System [USCS]), and specific gravity (G_s) of all the materials are provided in Table 5. Grain-size distribution curves of the materials are provided in Figure 9. Also included in Table 5 are the λ and S_r values determined following the Brooks and Corey *(35)* approach by developing SWCC curves using the Fredlund and Xing *(39)* model and empirical relationships provided in the earlier chapter.

TABLE 4 Description and source of materials

Material	Description	Lab/Field Study	Source
SAND 1	Concrete sand	Lab	Hallet Materials, Ames, IA
SAND 2	ASTM 20/30 silica sand	Lab	—
WLS-IA	Well-graded crushed limestone	Lab	Martin Marietta Materials, Ames, IA
PG	Open-graded pea gravel	Lab	Hallet Materials, Ames, IA
SGB	Small glass beads (0.75 mm spheres)	Lab	—
LGB	Large glass beads (1 mm spheres)	Lab	—
OLS-IA	Open-graded crushed limestone	Lab	Martin Marietta Materials, Ames, IA
OLS-63	Open-graded crushed limestone	Lab and Field	Hwy 63, New Hampton, IA
OS-MI	Open-graded slag	Lab and Field	I-94, Detroit, MI
#57-PA	AASHTO #57 crushed limestone†	Lab and Field	SR-22, Clyde, PA
OLS-PA	Open-graded crushed limestone	Lab and Field	SR-22, Clyde, PA

†used for cement-treated and asphalt-treated base.

TABLE 5 Summary of material index properties

Parameter	SAND1	SAND 2	OLS-IA	PG	WLS-IA	OLS-63	OS-MI	#57-PA	OLS-PA
Gravel (%) (> 4.75mm)	2	0	93	98	39	73	76	96	49
Sand (%) (4.75mm – 75μm)	96	100	6	2	50	17	17	3	41
Silt + Clay (%) (< 75μm)	2	0	1	0	11	11	7	1	10
D_{10} (mm)	0.28	0.64	4.88	8.05	0.06	0.07	0.30	6.84	0.08
D_{20} (mm)	0.43	0.70	5.29	9.60	0.27	2.99	3.73	8.75	0.71
D_{30} (mm)	0.57	0.74	5.68	10.82	0.60	5.22	6.09	10.21	1.70
D_{60} (mm)	1.20	0.77	6.92	14.48	4.66	11.52	13.60	14.46	6.66
D_{90} (mm)	3.00	0.80	8.60	20.73	10.65	22.83	28.68	21.86	21.30
c_u	4.2	1.2	1.4	1.8	77.6	167.1	44.8	2.11	74.1
c_c	1.0	1.0	1.0	1.0	1.3	34.2	9.0	1.1	4.8
AASHTO classification	A-1-b	A-1-a	A-1-a	A-1-a	A-1-a	A-1-a	A-1-a	A-1-a	A-1-a
USCS classification	SP	SP	GP	GP	SW-SM	GP-GM	GP-GM	GP	GP-GM

G_s	2.68	2.70	2.71	2.70†	2.68	2.76	2.87	2.70†	2.70†
λ	2.20	4.08	3.65	4.30	0.54	0.59	0.98	4.62	0.82
S_r (%)	10	10	5	2	11	15	12	2	11

†Assumed.

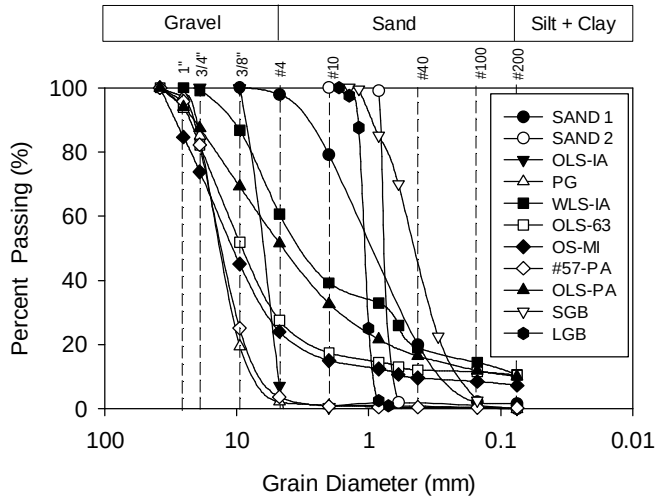

FIGURE 9 Grain-size distribution curves of materials

GPT REPEATABILITY AND MEASURMENT RANGE

Results obtained from repeated measurements on ten different material types using the GPT device setup with different orifice diameter sizes (GPT(A), GPT(B), GPT(C), and GPT(D)) are presented in this section. The materials were uniformly mixed and compacted in the laboratory in a 0.95 m diameter by 0.31 m height ring or a 0.57 m square by 0.15 m height box (Figure 10). The material thicknesses varied from about 0.08 to 0.30 m. The test procedure involved obtaining $P_{o(g)}$ measurements at five to ten different Q values on each material type. Then the K_{sat} is calculated corresponding to each Q value.

Repeated measurements obtained on all materials using the four GPT setups are presented in Figure 11. The K_{sat} measurement error ($\sigma_{repeatability}$) values were determined by performing two-way analysis of variance [ANOVA] considering the number of measurements and Q as random effects. The root mean squared error value resulted from the analysis is reported as the $\sigma_{repeatability}$ and is summarized in Table 6. COV values were calculated as the ratio of $\sigma_{repeatability}$ to the average K_{sat} value (for the K_{sat} range) and are summarized in Table 6. Analysis results indicate that excellent repeatability in the calculated K_{sat} (i.e., COV $\leq$ 1%) is achievable with a minimum $P_{o(g)}$ = 10 mm of H_20 and Q = 100 cm^3/s. For materials with relatively high hydraulic conductivity, achieving $P_{o(g)}$ = 10 mm of H_20 was not possible and the COV is in the range of 5 to 18%. For tests performed using GPT(D), achieving both a minimum $P_{o(g)}$ = 10 mm of H_20 and Q = 100 cm^3/s were not possible and the resulting COV value is 23%.

FIGURE 10 Laboratory GPT tests in 0.95 m diameter by 0.31 m height ring (left) and 0.57 m square by 0.15 m height box (middle), and large scale aggregate compaction mold laboratory permeameter [LSLP] tests (right)

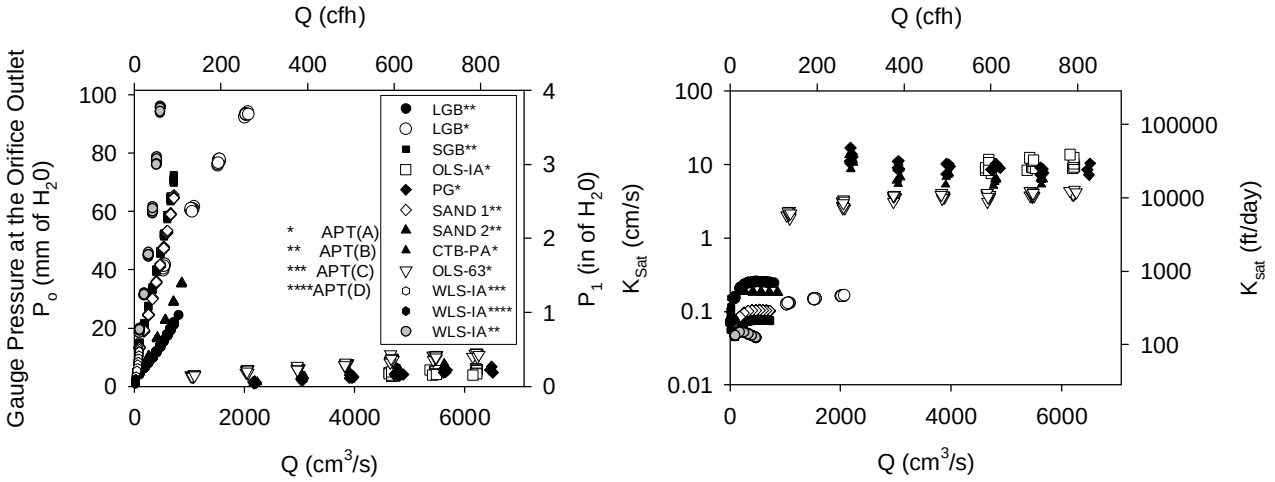

FIGURE 11 GPT repeatability on different materials [Note: P_1 (Pa) = P_o (mm of H_20)*250 + 101325]

TABLE 6 Repeatability of GPT K_{sat} measurements

Material	GPT ID	N	P_o Range (mm of H_20)	Q Range (cm^3/s)	K_{sat} Range (cm/s)	K_{sat} $\sigma_{repeatability}$ (cm/s)	COV (%)	Remarks
LGB	GPT(A)	47	39.8 to 94.3	520 to 2070	0.10 to 0.17	0.0001	≤ 1	Approximate target minimum: $P_{o(g)}$ = 10 mm of H_20 Q = 100 cm^3/s for COV ≤ 1%
SGB	GPT(B)	100	14.5 to 72.5	80 to 720	0.05 to 0.08	0.0004	≤ 1	
WLS-IA	GPT(B)	66	18.3 to 96.3	84 to 470	0.04 to 0.05	0.0004	≤ 1	
SAND1	GPT(B)	95	13.1 to 65.7	80 to 720	0.06 to 0.10	0.0005	≤ 1	
SAND2	GPT(B)	30	6.8 to 35.6	170 to 860	0.18 to 0.20	0.0014	≤ 1	
LGB	GPT(B)	99	4.1 to 21.9	80 to 720	0.15 to 0.26	0.0015	≤ 1	
WLS-IA	GPT(C)	70	3.0 to 15.1	30 to 105	0.06 to 0.07	0.0008	≤ 1	
OLS-63	GPT(A)	70	3.3 to 9.5	1020 to 6260	1.85 to 4.54	0.1857	5	$P_{o(g)}$ did not achieve the target minimum
OLS-IA	GPT(A)	21	3.5 to 6.1	4620 to 6260	7.59 to 13.62	1.3264	13	
PG	GPT(A)	26	1.0 to 6.7	2160 to 6500	7.19 to 16.94	1.5816	16	
CTB-PA	GPT(A)	24	1.1 to 7.9	1020 to 6260	5.16 to 14.53	1.3382	18	
WLS-IA	GPT(D)	19	0.8 to 2.7	12 to 25	0.05 to 0.15	0.0201	23	$P_{o(g)}$ and Q did not achieve the target minimum

The measurement ranges of GPT with four different orifice setups are presented in Figure 12. As a reference, typical K_{sat} range reported in the literature *(40)* for various soil types are also provided. The American Concrete Paving Association [ACPA] *(41)* recommends a target hydraulic conductivity of 0.02 to 0.04 cm/s for drainable bases. Hall et al. *(42)* reports that a hydraulic conductivity range of 0.12 to 0.53 cm/s is adequate for cement stabilized permeable bases. MEPDG *(4)* requires permeable bases have a minimum hydraulic conductivity of 0.35 cm/s.

For materials with relatively low hydraulic conductivity (K_{sat} < 0.01 cm/s), the GPT(C)(D) can be used by applying a "bleed off" correction. The "bleed off" correction procedure was an innovative discovery that greatly increases the measurement range for the device and has the potential to increase the use of the device for even lower hydraulic conductivity materials. In brief, this correction requires performing the following:

1. Place the GPT device on the base seal on a concrete impermeable surface and obtain $P_{o(g)}$ (over a range of 2.5 to 75 mm of H_20) and Q measurements with the controlled bleed-off valve open. Develop a linear relationship to estimate Q as a function of $P_{o(g)}$.

2. Using the same base seal, place the GPT device on the material surface and obtain $P_{o(g)}$ (over a range of 2.5 to 75 mm of H_20) and Q measurements. Using the relationship developed from step 1, estimate the Q values for the $P_{o(g)}$ values measured in step 2. Subtract the estimated Q values from step 1 from the measured Q values from step 2 to determine corrected Q values. Use the corrected Q values and $P_{o(g)}$ measured in step 2 in the K_{sat} calculation.

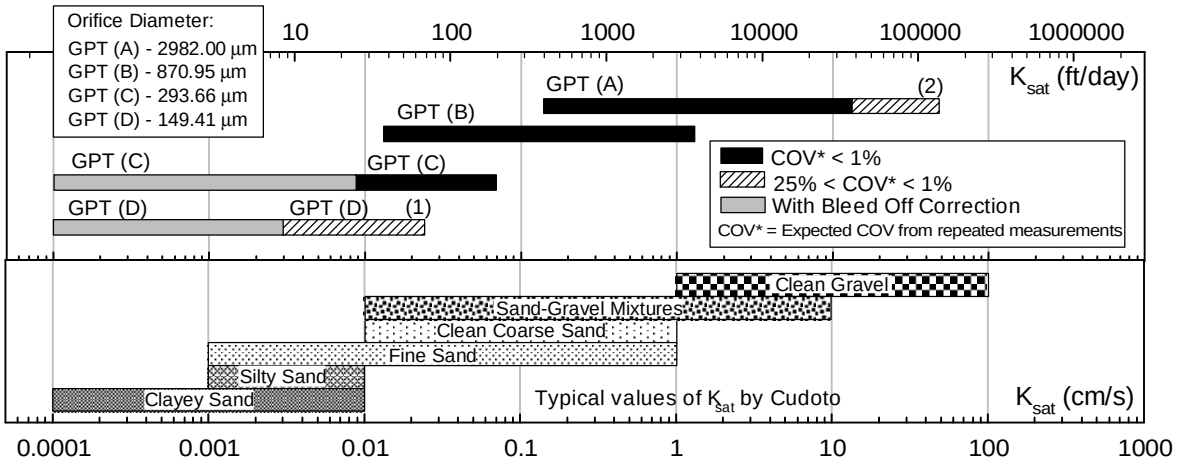

Notes:
(1) - With P_o < minimum recommended target of 10 mm of H_20)
(2) - With P_o < minimum recommended target of 10 mm of H_20 and Q < minimum recommended target of 100 cm^3/s

FIGURE 12 Measurement range of the GPT device using different orifice configurations

COMPARISON BETWEEN K_{SAT} DETERMINED FROM GPT, LABORATORY PERMEAMEABILITY TESTS, AND EMPIRICAL RELATIONSHIPS

GPT and laboratory hydraulic conductivity tests (using water) were conducted on 11 different materials (see Table 7) for comparison. GPT measurements were obtained on uniformly mixed and compacted materials in a 0.95 m diameter by 0.31 m height ring or a 0.57 m square by 0.15 m height box (Figure 10). The material thicknesses varied between 0.08 and 0.30 m. Laboratory hydraulic conductivity tests were conducted following ASTM D2434 constant head method test onmaterials (SGB and LGB). For the remaining materials, a specially fabricated 0.3 m diameter by 0.3 m high aggregate compaction mold LSLP (Figure 10) was used to perform falling head permeability tests. The details of the LSLP test procedure is described in White et al. *(8)*. Preparation of the test samples for the LSLP tests involved uniform mixing and compaction to a target dry unit weight (similar to GPT tests). The material thicknesses in the LSLP tests varied between 0.15 m and 0.30 m.

Results from the GPT and laboratory hydraulic conductivity measurements for all the materials are summarized in Table 7. The ratio of K_{sat} determined from GPT to laboratory hydraulic conductivity test varied from about 0.2 to 5.0. This variation between GPT and conventional laboratory measurements is attributed to the following:

1. The pressure head in the laboratory permeability tests (h_w) is in most cases significantly higher than the inlet gauge pressure ($P_{o(g)}$) in the GPT. The higher pressure head used in the laboratory permeability tests could cause non-laminar flow conditions for highly permeable materials.
2. During LSLP tests the direction of flow is one-dimensional (i.e., vertical), while the direction of flow in a GPT is three-dimensional. Also during GPT measurements, the gas flow passes through localized high permeable and low permeable zones beneath the device. Given that the more permeable pathways will control the drainage capacity, the GPT determined values would be expected to be higher than the laboratory measurements.

Based on these reasons above and the assumptions implicit to the K_{sat} derivation from GPT measurements, these differences between laboratory and GPT measurements are considered acceptable.

The empirical equation proposed by Moulton *(5)* and K_{sat} model used in the MEPDG EICM *(38)* as shown in equations 19 and 20, respectively, were also used to estimate K_{sat} for comparison with GPT measurements. Equation 19 was developed for granular base and subbase materials with $P_{200} > 0$ and therefore is applicable for eight out of eleven materials listed in Table 7. Equation 20 is developed for granular non-plastic soils with K_{sat} between 10^{-6} and 10^{-2} cm/s

(note that this correlation is based on limited measurements and showed significant scatter in the data) and is applicable for three out of eleven materials listed in Table 7.

$$K_{sat}\ (\text{ft/day}) = \frac{6.214\times10^{5}\, D_{10}^{1.478}\, n^{6.654}}{P_{200}^{0.597}} \quad (19)$$

$$K_{sat}\ (\text{cm/s}) = 10^{-6}\times10^{\left(5.3D_{10}+0.049D_{60}+0.0092\frac{D_{60}}{D_{10}}-0.1P_{200}+1.5\right)} \quad (20)$$

TABLE 7 Summary of comparison between laboratory permeability tests, GPT measurements, and empirical estimations

Material	Laboratory Permeability Test Measurements			GPT Measurements				Ratio of GPT and lab K_{sat} (cm/s)	Empirically estimated K_{sat} (cm/s)
	Range of h_w (mm)	γ_d (kN/m^3)	K_{sat} (cm/s)	Range of $P_{o(g)}$ (mm)	Range of Q (cm^3/s)	γ_d (kN/m^3)	K_{sat} (cm/s)		
WLS-IA	900 to 620	19.05	3.5E-04†	53 to 77	22 to 30	18.90	4.4E-04***	1.3	1.8E-04‡, 4.6E-05‡‡
SAND 1	900 to 600	17.96	0.02†	13 to 65	80 to 720	17.60	0.10**	5.0	0.01‡, 7.62E-04‡‡
OLS-PA	900 to 500	19.50	0.08†	—§					1.9E-04‡, 1.0E-04‡‡
SGB	360 to 50	14.77	0.16††	15 to 73	80 to 720	14.78	0.07**	0.4	NA‡, NA‡‡
LGB	170 to 50	15.57	0.59††	4 to 22	520 to 2070	15.56	0.13*	0.2	NA‡, NA‡‡
				40 to 94	520 to 2070	15.56	0.24**	0.4	
OLS-63	900 to 500	15.92	1.47†	3 to 12	1020 to 6260	16.45	4.16*	2.8	2.1E-03‡, NA‡‡
CTB	177 to 51	17.03	1.53†	5 to 15	1020 to 6260	16.73	6.49*	4.2	4.9‡, NA‡‡
PG	900 to 500	15.15	2.17†	1 to 7	2160 to 6500	16.12	9.69*	4.5	NA‡, NA‡‡
OLS-IA	900 to 500	17.35	2.89†	4 to 6	4620 to 6260	17.40	10.09*	3.5	1.9‡, NA‡‡
OS-MI	900 to 500	14.77	3.14†	< 1 to 6	1040 to 6260	14.77	11.49*	3.7	0.08‡, NA‡‡
ATB	900 to 700	—§	6.46†		—§				4.9‡, NA‡‡

*GPT(A), **GPT(B), ***GPT(C), †Laboratory permeability tests using LSLP, ††Laboratory permeability tests following ASTM D2434 procedure, §Not measured, ‡calculated using equation 8, ‡‡calculated using equation 9, NA-not applicable.

Equation 19 produced estimates that are within one order of magnitude variation for five materials (WLS-IA, SAND 1, CTB, OLS-IA, and ATB) and greater than two orders of magnitude variation for three materials (OLS-PA, OLS-63, and OS-MI). Equation 20 produced an estimate that is within one order of magnitude variation for one material (WLS-IA) and estimates that are greater than three orders of magnitude variation for two materials (SAND1, OLS-PA). While empirical estimates are relatively simple to use, they are not always effective because: (a) the relationships are valid only for a certain range of measurements, (b) gradation properties cannot be rapidly determined to capture the variations observed in-situ (note that previous field studies indicated significant variation of fines content on granular base and subbase layers (*33*)), and (c) the relationships often have significant scatter in the data and may not provide a statistically reliable estimate of K_{sat}.

INFLUENCE OF PARTIAL SATURATION ON K_{SAT} DETERMINED FROM GPT

To assess the influence of partial saturation on the calculated K_{sat} from GPT measurements, SAND1 and SAND2 materials were tested at different degrees of saturation (S = 0 to 70%). The test procedure involved uniformly mixing the materials (using a soil mixer) to a target moisture content and compacting the materials to a target dry unit weight (SAND 1 target γ_d =16.65 kN/m^3 and SAND 2 target γ_d =16.38 kN/m^3) in a 0.57 m square by 0.15 m height box (Figure 13). The material thickness was kept constant at about 10 cm.

The results obtained from this series of tests are presented in Figure 14. Variation in γ_d between tests was inevitable. Therefore, multiple regression analysis was performed to assess the influence of variations in γ_d and S on the calculated K_{sat} values (Figure 14). Statistical significance of each variable was assessed using *p*-value and *t*-ratio results from the analysis. The *p*-value indicates the significance of a variable and the *t*-ratio value indicates the relative importance (i.e., higher the absolute value greater the significance). Commonly, variables with *p*-value < 0.05 and *t*-ratio < -2 or > +2

are considered statistically significant. Based on these criteria, for SAND 1 – S is significant while γ_d is not significant and for SAND 2 – both S and γ_d are significant. However, for SAND2 the *t*-ratio for S (i.e., 4.91) is greater than the *t*-ratio for γ_d (i.e., 2.76) which indicates that S has a relatively greater statistical significance than γ_d in the multiple regression models.

For the two materials tested, increasing S resulted in an increase in the calculated K_{sat} especially at S > 30%. This suggests that at higher degrees of saturation the calculated K_{sat} value results in a slight overestimation (less than one order of magnitude for S = 40% to 70%). Factors that partially contribute to this overestimation include: (a) change in material degree of saturation during testing due to material drying (see picture in Figure 13) thus causing a decrease in degree of saturation (note that a decrease in S causes a decrease in K_{sat} as shown in Figure 14); and (b) unquantified effect of water particle movement due to pressurized gas flow in the soil.

FIGURE 13 Pictures showing compaction (left) and testing (middle) process on materials at different degrees of saturation and a picture showing dry material at the surface that is in contact with the orifice outlet after testing with GPT device (right)

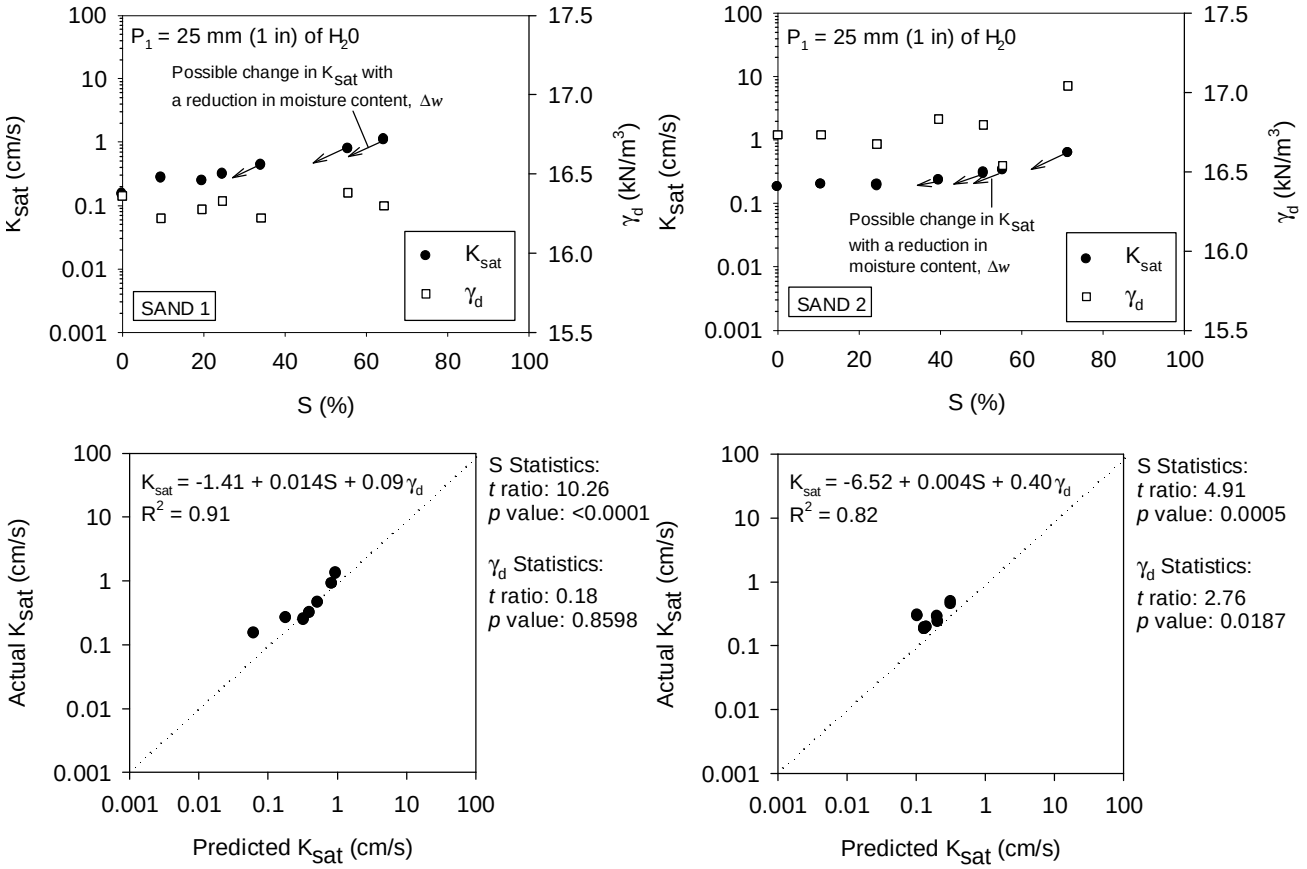

FIGURE 14 Influence of partial saturation on estimated K_{sat} from GPT measurements

FIELD STUDIES

Field testing was conducted at three project sites with new pavement base/subbase layer construction in Iowa, Michigan, and Pennsylvania. The base and subbase materials varied from open-graded crushed limestone to open-graded steel slag to cement-treated/asphalt-treated open graded crushed limestone. In situ testing involved conducting both GPT and moisture-dry unit weight tests at 70 to 120 locations within 40 to 200 m^2 test areas. Bag samples of untreated base materials were obtained and transported to laboratory to determine moisture content and fines content (passing # 200 sieve). Results from such dense testing allowed for assessing spatial variability using geostatistical semivariogram analysis. Additional details on spatial variability analysis, results from field testing, influence of fines content on K_{sat}, and comparison between laboratory and field measurements are discussed below.

SPATIAL VARIABILITY ASSESSMENT USING SEMIVARIOGRAM ANALYSIS

Spatial variability can be assessed and quantified using geostatistical semivariogram analysis. The semivariogram $\gamma(h)$ is defined as one-half of the average squared differences between data values that are separated at a distance h *(49)*. If this calculation is repeated for as many different values of h as the sample data will support, the result can be graphically presented as shown in Figure 15 (shown as circles), which constitutes the experimental semivariogram plot. The mathematical expression to estimate the experimental semivariogram is also provided in Figure 15 where $z(x_i)$ is a measurement taken at location x_i, and n(h) is the number of data pairs h units apart in the direction of the vector. A theoretical model can be fit to the experimental semivariogram to give an algebraic formula defining the spatial relationship between values at specified distances. There are many possible models to fit an experimental semivariogram. Some commonly used models include spherical, exponential, and Gaussian models. Spherical model is used for all the results presented in this report. The mathematical expression for the spherical model is provided in Figure 15. The three main parameters that define a model include the range (a), sill ($C+C_0$), and nugget (C_0) as defined in Figure 15. An important to note in semivariogram modeling is that a model is stable only if the measurement values are stationary (i.e., normally distributed) over an aerial extent. If the data values are non-stationary (i.e., binomially distributed or skewed), spatial variability should be modeled only after appropriate transformation of the data *(50)*. Previous experience *(33)* and results from this study showed that hydraulic conductivity values typically show skewed distributions and require a log transformation for semivariogram modeling. In addition to quantifying spatial variability, geostatistics can be used as a spatial prediction technique, i.e., for predicting values at unsampled locations based on values at sampled locations. Kriging is a stochastic interpolation procedure *(51)* by which the variance of the difference between the predicted and "true" values is minimized using a semivariogram model. Kriging is used to create "smoothed" contour maps of field measurements and are presented in the following sections.

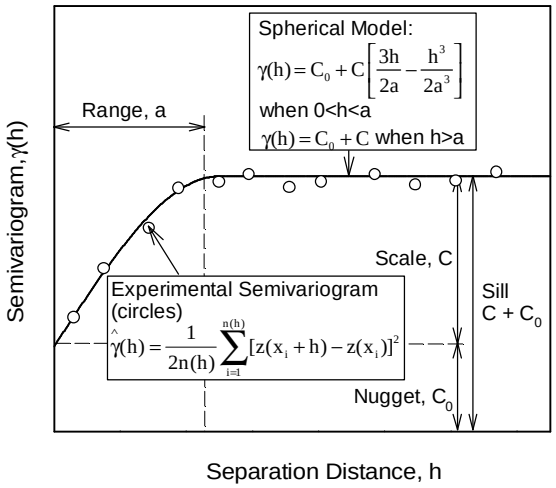

Range: As the separation distance between pairs increase, the corresponding semivariogram value will also generally increase. Eventually, however, an increase in the distance no longer causes a corresponding increase in the semivariogram, i.e., where the semivariogram reaches a plateau. The distance at which the semivariogram reaches this plateau is called as range. Longer range values suggest greater spatial continuity or relatively larger (more spatially coherent) "hot spots".

Sill: The plateau that the semivariogram reaches at the range is called the sill. A semivariogram generally has a sill that is approximately equal to the variance of the data.

Nugget: Though the value of the semivariogram at h = 0 is strictly zero, several factors, such as sampling error and very short scale variability, may cause sample values separated by extremely short distances to be quite dissimilar. This causes a discontinuity at the origin of the semivariogram and is described as nugget effect. (Isaaks and Srivastava, 1989)

FIGURE 15 Typical semivariogram plot and its characteristics

Project No. 1: Open-Graded Crushed Limestone, Highway 63, New Hampton, Iowa

This project involved testing on a newly constructed pavement base layer on Highway 63 near New Hampton, Iowa. The base layer consisted of a nominal 200 mm thick compacted and trimmed open-graded crushed limestone material (OLS-63 USCS classification: GP-GM; AASHTO classification: A-1-a) underlain by relatively impervious subgrade. Index properties of the base material are summarized in Table 5. Field testing involved GPT (using GPT(B)) measurements at 89 test locations in a grid pattern within a 9 m by 4 m test area. Due to weather constraints, moisture and dry unit weight measurements using nuclear gauge were obtained at only 17 randomly selected test locations in the grid. GPT measurements were obtained at various combinations of $P_{o(g)}$ and Q measurements over a range of 5 to 75 mm of H_20 and 200 to 700 cm^3/s, respectively. An average K_{sat} was calculated for different combinations of $P_{o(g)}$ and Q at each test location. Following GPT measurements, bag samples of the base materials from directly beneath the GPT location were obtained for moisture content and percent fines tests. Material saturation at each test location was calculated using average in situ dry unit weight (γ_d = 16.76 kN/m^3) and moisture content measurements from bag samples for K_{sat} calculation. The λ and S_r values used for K_{sat} calculation are summarized in Table 5. A summary of univariate and spatial statistics of K_{sat}, fines content, dry unit weight, moisture content, and degree of saturation measurements are presented in Table 8. Spatial contour maps, semivariogram plots with spatial statistics, histogram plots with univariate statistics of fines content and K_{sat} are presented in Figure 16.

Project No. 2: Open-Graded Crushed Steel Slag, Interstate-94, Detroit, Michigan

This project involved testing a newly constructed pavement base layer on Interstate 94 just north of Detroit, Michigan. The base layer consisted of a nominal 400 mm thick compacted and trimmed open-graded crushed steel slag material (OS-MI USCS classification: GP-GM; AASHTO classification: A-1-a) underlain by relatively impervious subgrade. Index properties of the base material are summarized in Table 5. Field testing involved obtaining GPT (using GPT(B)) measurements and moisture-dry unit weight measurements using nuclear gauge measurements at 120 test locations in a grid pattern over a 7 m by 7 m test area. GPT measurements were obtained at various combinations of $P_{o(g)}$ and Q measurements over a range of 1 to 75 mm of H_20 and 250 to 600 cm^3/s, respectively. An average K_{sat} was calculated for different combinations of $P_{o(g)}$ and Q at each test location. Following GPT measurements, bag samples of the base materials from directly beneath the GPT location were obtained for moisture content and percent fines tests. The λ and S_r values used for K_{sat} calculations are summarized in Table 5. A summary of univariate and spatial statistics of K_{sat}, fines content, dry unit weight, moisture content, and degree of saturation measurements are presented in Table 8. Spatial contour maps, semivariogram plots with spatial statistics, histogram plots with univariate statistics of fines content and K_{sat} are presented in Figure 17.

Project No. 3: Stabilized Open-Graded Base, SR-22, Pennsylvania

This project involved testing newly constructed cement-treated open-graded crushed AASHTO#57 stone base [CTB], asphalt-treated AASHTO#57 stone base [ATB], and open-graded crushed limestone leveling subbase [OLS-PA] layers on SR-22 near Blairsville, Pennsylvania. The gradation properties of the AASHTO#57 stone [#57-PA] and the OLS-PA subbase materials are summarized in Table 5.

Project 3a involved testing on the CTB layer. The CTB layer was approximately 100 mm thick underlain by 50 mm thick crushed limestone leveling subbase and 450 mm of rock cap. The section of the CTB tested was located on connected shoulder lanes of the eastbound and westbound lanes (see Figure 18). The eastbound lane base layer was constructed in summer 2009 while the westbound lane base layer was constructed in fall 2008. A portion of the westbound lane base layer [Area B] was contaminated with washed out fines (see Figure 18). Field testing involved obtaining GPT measurements and moisture-dry unit weight measurements using nuclear gauge at 49 locations in Area A and 23 measurements in Area B. GPT(A) was used in Area A with relatively high hydraulic conductivity and GPT(B) was used in Area B with relatively low hydraulic conductivity. The total test area combining Areas A and B was about 5 m by 9 m. GPT measurements were obtained at various combinations of $P_{o(g)}$ and Q measurements over a range of 5 to 75 mm of H_20 and 250 to 7500 cm^3/s, respectively. An average K_{sat} was calculated for different combinations of $P_{o(g)}$ and Q at each test location. The λ and S_r values determined for #57-PA material are provided in Table 5. A summary of univariate and spatial statistics of K_{sat}, fines content, dry unit weight, moisture content, and degree of saturation measurements are presented in Table 8 separately for Area A and Area B. Spatial contour maps, semivariogram plots with spatial statistics, histogram plots with univariate statistics of fines content and K_{sat} are presented in Figure 18.

Since the combined K_{sat} data obtained from Areas A and B is non-stationary, i.e., binomially distributed, the two areas were separately modeled in the semivariogram analysis. Kriged contours are generated separately for the two areas using the respective semivariogram models and then combined as presented in Figure 18.

Project 3b involved testing ATB and leveling subbase layers. The ATB layer was approximately 100 mm thick underlain by 50 mm of leveling subbase and 450 mm of rock cap. The area tested consisted of ATB layer on the mainline and exposed leveling subbase layer in the shoulder Figure 19. Field testing involved GPT and nuclear gauge measurements at 99 test locations in an area of about 14 m by 14 m. GPT(A) was used on the ATB layer and GPT(B) was used on the leveling subbase layer. GPT measurements were obtained at various combinations of $P_{o(g)}$ and Q measurements over a range of 5 to 75 mm of H_20 and 200 to 7500 cm^3/s, respectively. An average K_{sat} was calculated for different combinations of $P_{o(g)}$ and Q at each test location. The λ and S_r values determined for #57-PA and #OLS-PA materials are provided in Table 5. A summary of univariate and spatial statistics of K_{sat} and dry unit weight measurements are presented in Table 8. Spatial contour maps, semivariogram plots with spatial statistics, histogram plots with univariate statistics of K_{sat} are presented in Figure 19. The ATB layer and leveling base layer contained different ranges of K_{sat} thus presenting non-stationary conditions; therefore, the two areas were separately modeled in the semivariogram analysis. Kriged contours are generated separately for the two areas using the respective semivariogram models and then combined as presented in Figure 19.

TABLE 8 Summary statistics of field measurements

Parameter	Project No. 1	Project No. 2	Project No. 3a		Project No. 3b
Material	Crushed Limestone (OLS-63)	Steel slag (OS-MI)	Cement treated AASHTO # 57 base (CTB)		Asphalt treated AASHTO#57 base (ATB)
			Area A	Area B	
Saturated Hydraulic Conductivity, K_{sat} Statistics					
Number of measurements, N	89	120	49	23	99
Mean, μ (cm/s)	1.9	4.9	7.0	0.2	4.6
Standard Deviation, σ (cm/s)	1.7	5.9	3.1	0.2	1.9
Coefficient of Variation, COV (%)	91	119	45	101	42
Variogram Sill, $C+C_0$	0.15	0.34	0.08	0.04	0.03
Variogram Range, a (m)	1.5	2.3	3.0	2.5	4.0
Fines Content Statistics					
Number of measurements, N	87	120			
Mean, μ (%)	10.5	3.7			
Standard Deviation, σ (%)	2.5	1.4	No Measurements		No Measurements
Coefficient of Variation, COV (%)	24	37			
Variogram Sill, $C+C_0$	5.8	2.0			
Variogram Range, a (m)	2.0	1.8			
Dry Unit Weight, g_d Statistics					
Number of measurements, N	17	120	49	23	99
Mean, μ (kN/m^3)	17.76	20.01	16.98	18.50	17.64
Standard Deviation, σ (kN/m^3)	0.52	0.62	2.25	0.75	1.88
Coefficient of Variation, COV (%)	3	3	13	4	11
Moisture Content Statistics					
Number of measurements, N	89	120	49	23	
Mean, μ (%)	6.8	3.3	6.2	6.1	Not Applicable
Standard Deviation, σ (%)	2.2	0.6	0.6	0.7	
Coefficient of Variation, COV (%)	33	20	10	11	
Degree of Saturation, S Statistics					
Number of measurements, N	17	120	49	23	Not Applicable
Mean, μ (%)	36	24	31	38	
Standard Deviation, σ (%)	7	6	6	4	

Coefficient of Variation, COV (%)	19	24	18	11	

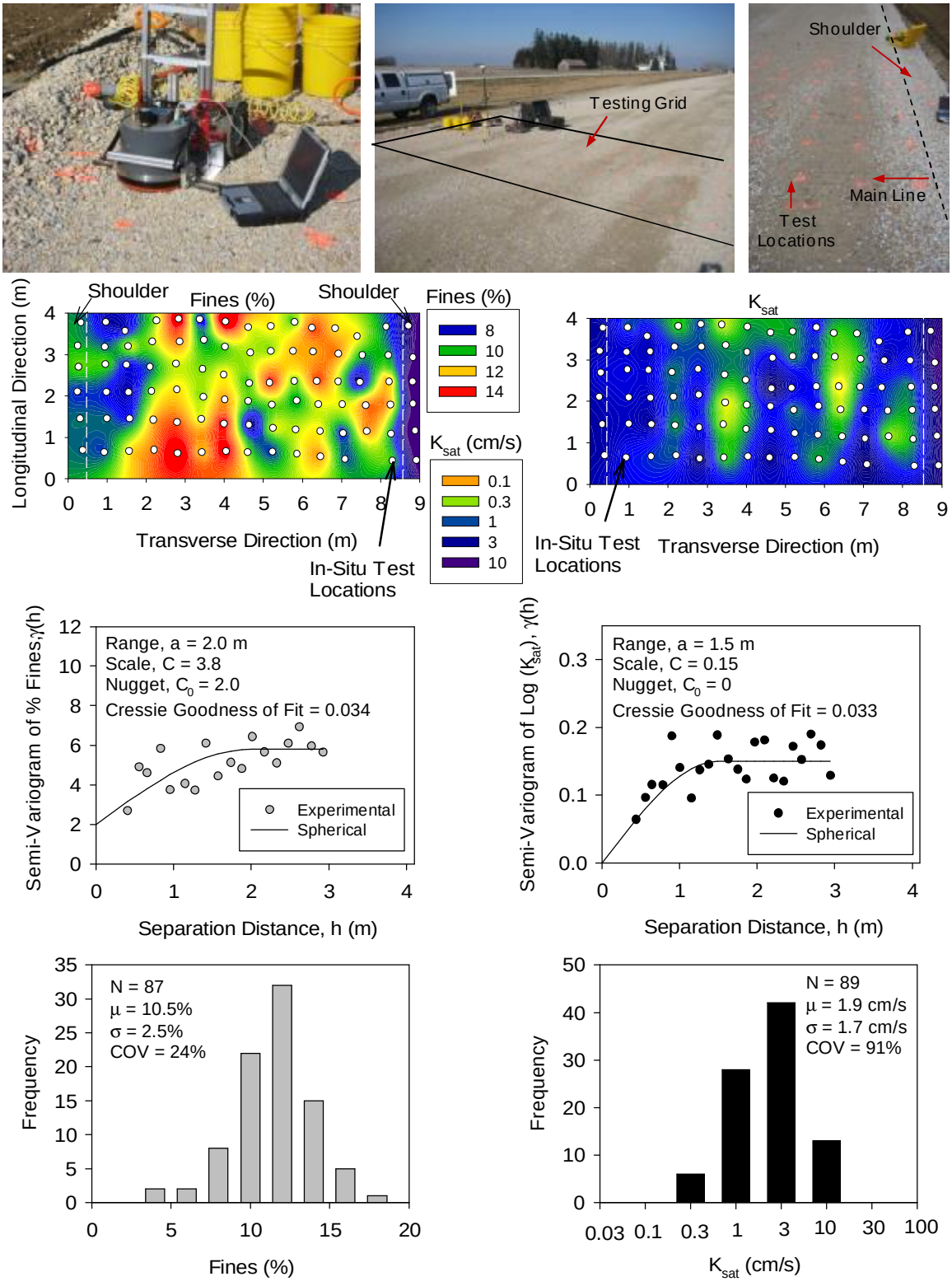

FIGURE 16 Photographs of testing and Kriged spatial maps (top), semivariograms (middle), and histogram plots (bottom) of fines content and K_{sat} on compacted permeable base on Highway 63, New Hampton, Iowa

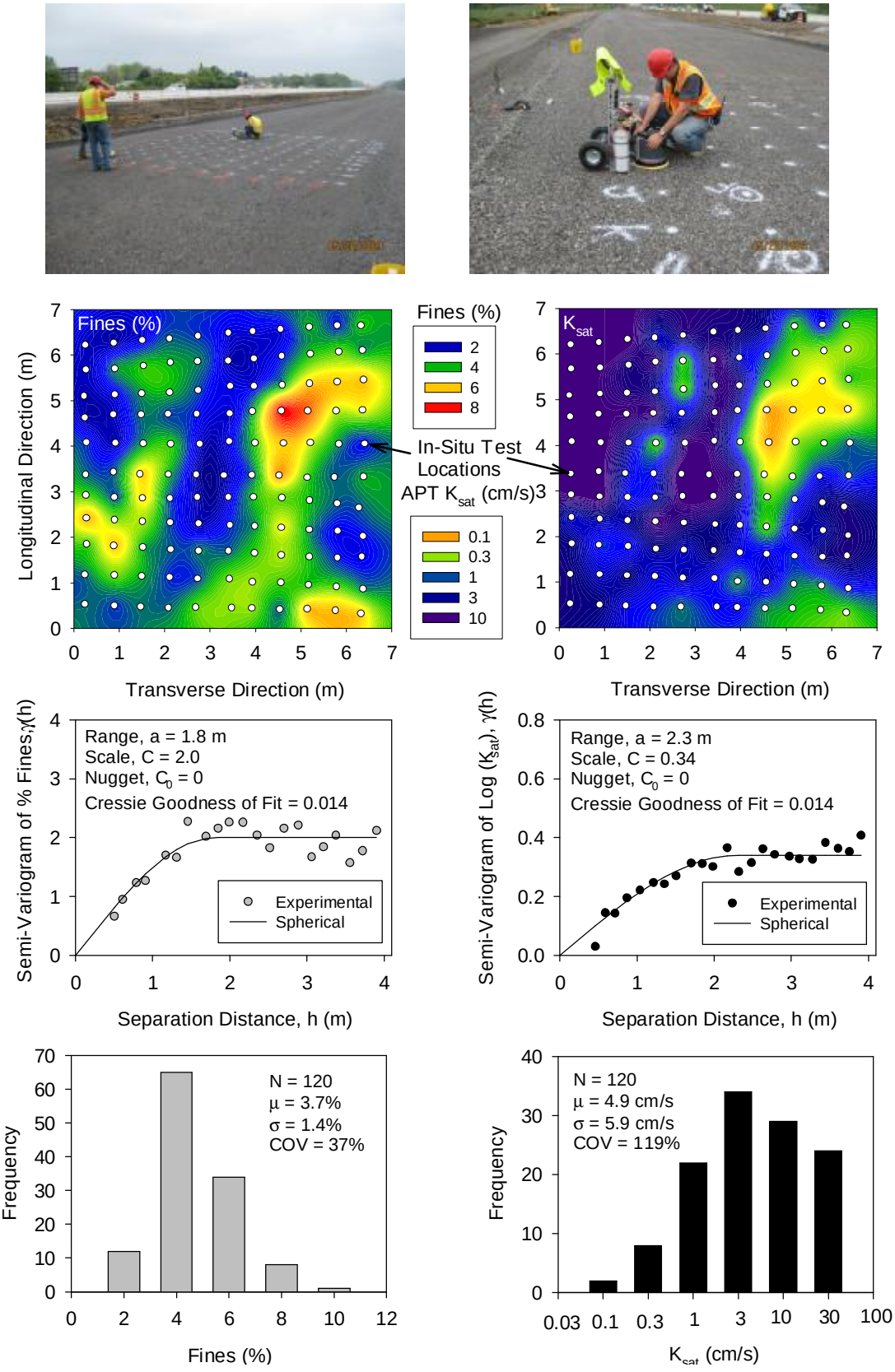

FIGURE 17 Photographs of in-situ testing and Kriged spatial maps (top), semivariograms (middle), and histogram plots (bottom) of fines content and K_{sat} on compacted open-graded steel slag base on I-94 project, Michigan

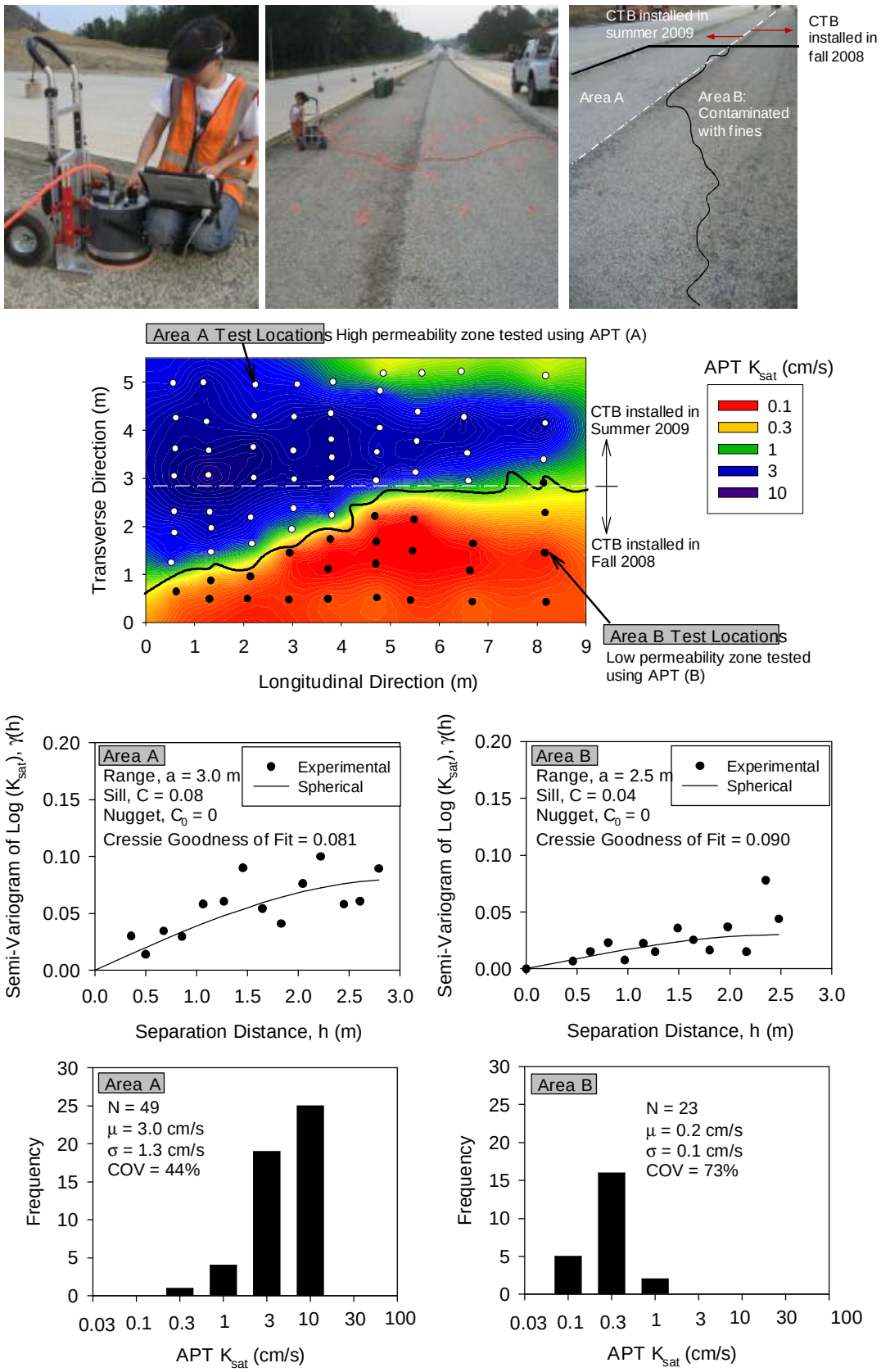

FIGURE 18 Kriged spatial map (top), semivariograms (middle), and histogram plots (bottom) of APT K_{sat} on cement treated base on SR-22 project near Clyde, Pennsylvania

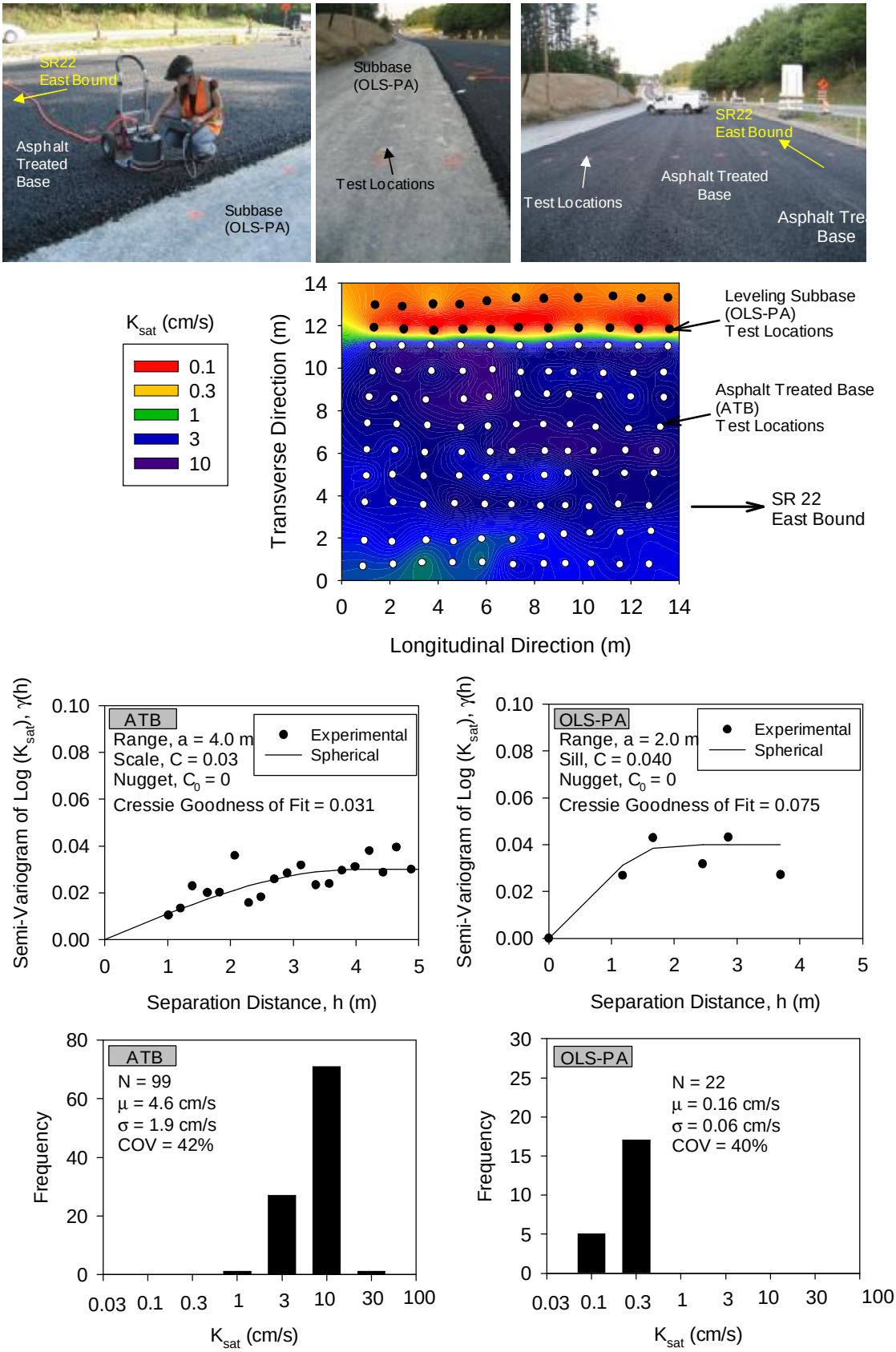

FIGURE 19 Kriged spatial map (top), semivariograms (middle), and histogram plots (bottom) of K_{sat} on asphalt treated base and leveling subbase on SR-22 project near Blairsville, Pennsylvania

INFLUENCE OF FINES CONTENT ON IN-SITU K_{SAT} MEASUREMENTS

Saturated hydraulic conductivity of granular materials is highly governed by its gradation; particularly the fines passing # 200 sieve *(5).* AASHTO *(3)* reports a decrease in saturated hydraulic conductivity of unbound granular drainage materials by two orders of magnitude with an increase in fines from 0 to 5%, and decrease by about four orders of magnitude with an increase in fines from 5 to 10%. Relationships between fines content on K_{sat} based on measurements obtained from the field projects described above are presented in Figure 20. Exponential relationships showed the best fit for the trends in the data. A similar relationship is reported in previous studies *(33)* and is included in Figure 20 for reference. Based on the R^2 values, about 20 to 60% of the variation in K_{sat} is explained by the variation in fines content. Other parameters that influence K_{sat} include other gradation parameters (e.g., D_{10}, D_{60}, etc.), shape and orientation of aggregate particles and dry unit weight, as expected.

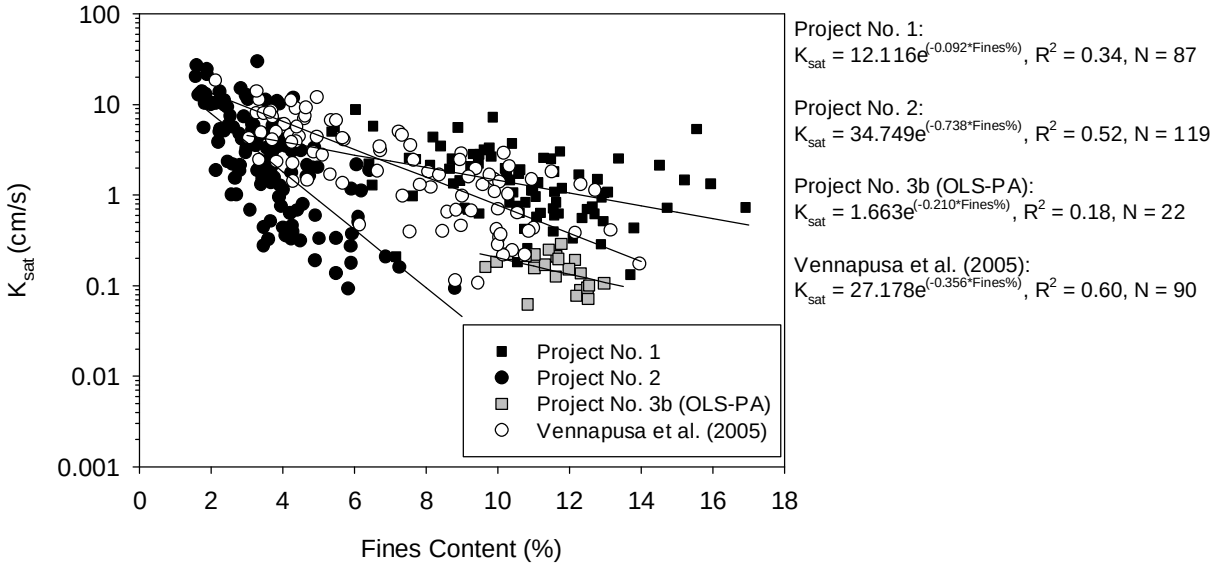

FIGURE 20 Effect of fines content on in-situ K_{sat}

KEY OBSERVATIONS FROM FIELD TESTING

Some key observations from the field testing exercise and analysis are as follows:

- Spatial maps developed from dense sampling as shown in Figure 16 to Figure 19 could be used as QA/QC criteria during base/subbase placement, grading, and compaction to identify field problems such as segregation and particle degradation.
- Visual interpretation of fines content and K_{sat} spatial maps for all project sites showed a good match between zones of high fines content with low hydraulic conductivity and vice versa.
- Regression analysis between fines content and K_{sat} indicated that about 20 to 60% of the variation in K_{sat} is explained by the variation in fines content.
- Summary statistics presented in Table 8 indicate that field K_{sat} measurements on crushed limestone and steel slag materials (Project No. 1 and 2) showed more variability (COV = 91 to 110%) than on cement-treated and asphalt treated base materials (Project No. 3a (Area A) and Project No. 3b: COV = 42 to 45%). Project No. 3a with cement-treated base material contained a portion (Area B) which was contaminated with washed out fines and showed a K_{sat} value that is on average about 35 times lower than Area A which was not contaminated with fines. This observation is important to note as permeable base layers must be properly maintained post construction.
- Project No. 1 OLS-63 material showed a laboratory K_{sat} value of about 4.2 cm/s (see Table 7) while K_{sat} in-situ varied from about 0.1 to 8.8 cm/s. Project No. 2 OS-MI material showed a laboratory K_{sat} value of about 6.5 cm/s (see Table 7) while K_{sat} in-situ varied from about 0.1 to 30.1 cm/s. Project No. 3a CTB material showed a laboratory K_{sat} value of about 11.5 cm/s (see Table 7) while K_{sat} in-situ varied from about 0.1 to 18.3 cm/s. Project No. 3b ATB material showed a laboratory K_{sat} value of about 6.5 cm/s (see Table 7) while K_{sat} in-situ

varied from about 1.3 to 10.6 cm/s. Comparison between laboratory and field measurements are presented as box plots in Figure 21.

- Spatial statistics summarized in Table 8 indicate that better spatial uniformity of K_{sat} on cement-treated and asphalt-treated base materials is reflected with the lower sill and longer range values compared to on crushed limestone and steel slag materials. Although limited data, the data suggests that particle segregation and degradation during construction can be better controlled with stabilized/treated materials than with untreated materials.

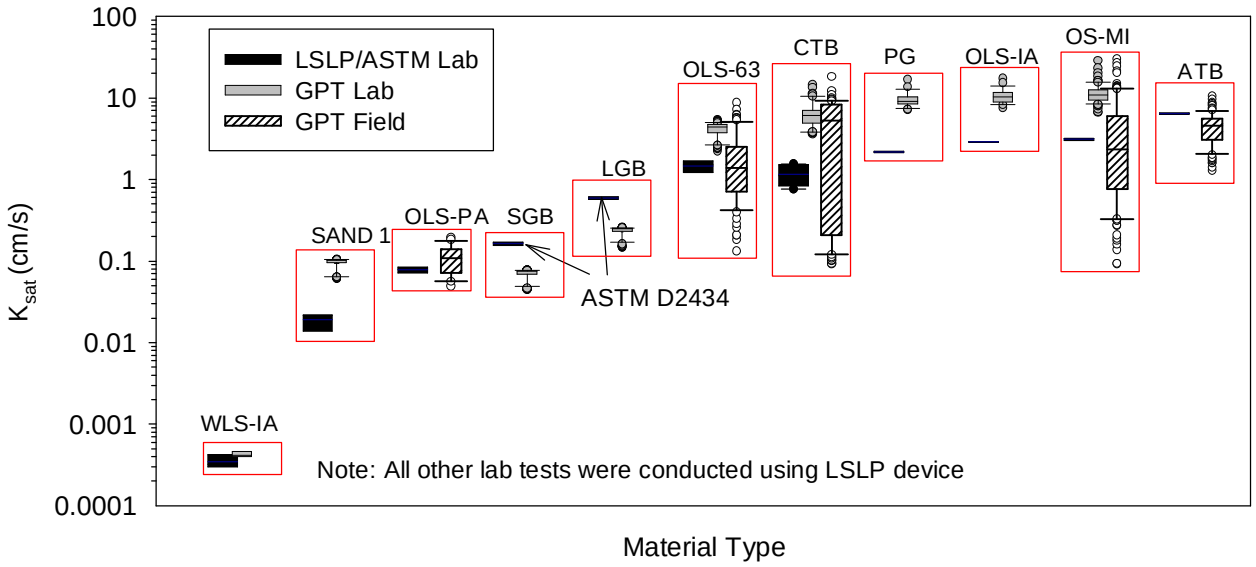

FIGURE 21 Comparison of saturated hydraulic conductivity determined from large-scale laboratory permeability/ASTM D2434 test measurements using water, APT measurements in lab, and APT measurements in field

CONCLUDING REMARKS

This research study contributed to successfully build and validate a rapid in-situ permeability testing device to determine saturated hydraulic conductivity (K_{sat}) of pavement base/subbase materials. The test device provides a repeatable measurement with rapid results (less than 30 seconds). By using this device, multiple tests can be performed in the field in a short period of time over a small area allowing for spatial analysis of the results which can be used as QA/QC criteria to identify field problems such as segregation and particle degradation. The device is also applicable for field QA/QC of pervious pavement materials. In-situ permeability measurements will allow for greater precision in design, construction and field QC/QA. Because of the large cost of projects involving pavement systems, even a small percent on over design or improved long-term performance due to improved uniformity could pay for a large amount of testing.

State DOTs and contractors will be able to utilize the findings from this research study as guidance for making informed decisions about how pavement base/subbase construction and specifications can be used to improve construction operations (e.g. spreading, compaction, and trimming operations). With increasing interest in moving towards performance-based and performance-related specifications, the device can be used as an effective in-situ QA tool to verify the design assumptions. State agencies can primarily implement the product through letting of projects with use of the device and specifications. Field target values and target limits can be included as part of the QA/QC specifications based on the findings presented in this report.

The discussion that follows provide some strategies to move forward for implementation of the device into QA/QC practice, some limitations to address as part of future research work.

IMPLEMENTATION STRATEGIES

The authors' are working with Handy Geotechnical Instruments, Inc. [HGI, Inc.] (www.handygeotech.com) to make the product commercially available. The mission of this company is to invent, develop and market geotechnical test instruments for direct in-situ measurement of relevant soil properties.

Some other future implementation strategies could involve: (a) dissemination of research results at workshops (some preliminary results from this research are presented at a poster presentation session in the 2009 Annual Transportation Research Board [TRB] meeting in Washington, D.C.), conferences, and by publishing in peer-reviewed journals; (b) national level demonstration projects through stated/federal pooled funded studies; and (c) training/certification program.

LIMITATIONS AND RECOMMENDATIONS FOR FUTURE RESEARCH

Based on the outcomes of this study, recommendations for future research are as follows:

- The GPT current design has a setup to manually change the orifice size depending on the hydraulic conductivity of the materials – smaller orifice size needed with low hydraulic conductivity materials. An advancement to this would be a design that is equipped with multiple orifices connected in different channels to the outlet that allows for automatically switching the channels based on the pressure-flow relationships.
- The GPT validation procedures described in this report with large scale laboratory hydraulic conductivity testing involved water heads that are significantly greater than the inlet pressures applied during the GPT test. Future work with a horizontal laboratory permeameter that allows maintaining water head levels that are similar to the GPT test (i.e., < 75 mm) would be a better comparison with GPT measurements.
- Limited laboratory testing conducted on two sand materials indicated that the K_{sat} estimated following Brooks and Corey *(35)* approach of accounting for partial saturation, results in an overestimation of K_{sat} (on the order of 2 to 5 for an increase in degree of saturation from 40% to 70%) with increasing material degree of saturation. Factors identified that partially contribute to this overestimation include: (a) change in material degree of saturation due to material drying during test, thus causing a decrease in degree of saturation; and (b) unquantified effect of water particle movement due to pressurized gas flow in the soil. Future work may involve laboratory testing monitoring the drying curve of the material due to the gas pressures applied, and gas flow modeling to study water movement due to pressurized flow in partially saturated porous media to gain further understanding on how to better account for partial saturation in K_{sat} estimation.
- Although this research project resulted in a validated and functional device, to fully implement this technology, detailed specifications, a manufacturer to supports the device, field training, and pilot projects are needed.

GLOSSARY

a	=	Range (semivariogram)
a_f, a_i	=	SWCC curve fitting parameter
b, b_f	=	SWCC curve fitting parameter
c, c_f	=	SWCC curve fitting parameter
C	=	Scale (semivariogram)
C_0	=	Nugget (semivariogram)
c_u	=	Coefficient of uniformity
c_c	=	Coefficient of curvature
CF	=	Correction factor in flow rate calculation from precision orifice measurements
d	=	Orifice diameter
D_0, D_{100}	=	SWCC curve fitting parameters
D_{10}	=	Particle diameter at which 10% of the particles present are finer
D_{20}	=	Particle diameter at which 20% of the particles present are finer
D_{30}	=	Particle diameter at which 30% of the particles present are finer
D_{60}	=	Particle diameter at which 60% of the particles present are finer
D_{90}	=	Particle diameter at which 90% of the particles present are finer
g	=	acceleration due to gravity
G_o	=	Geometric factor used in K_{sat} calculation
G_s	=	Specific gravity
h	=	Separation distance (in semivariogram)
h_w	=	Water pressure head
m_1, m_2	=	SWCC curve fitting parameters
M	=	Molecular weight of gas
n	=	porosity
N	=	Number of samples
K_{sat}	=	Saturated hydraulic conductivity
K_{gas}	=	Gas permeability
K_{rg}	=	Relative permeability to gas
$P_{i(a)}$	=	Absolute pressure at the orifice inlet
$P_{i(g)}$	=	Gauge pressure at the orifice inlet
$P_{o(a)}$	=	Absolute pressure at the orifice outlet
$P_{o(g)}$	=	Gauge pressure at the orifice outlet
P_1	=	Absolute gas pressure on the soil surface
P_2	=	Atmospheric pressure
P_{200}	=	Percent fines passing # 200 sieve
PI	=	Plasticity index
Q	=	Volumetric flow rate
r	=	radius at outlet orifice
S	=	Degree of water saturation
S_e	=	Effective water saturation
S_r	=	Residual water saturation
T	=	Temperature
$\gamma(h)$	=	Semivariogram
γ_d	=	Dry unit weight
λ	=	Brooks-Corey pore size distribution index
μ	=	Statistical mean
μ_{gas}	=	Kinematic viscosity of gas
μ_{water}	=	Absolute viscosity of water
σ	=	Statistical standard deviation
$\sigma_{repeatability}$	=	Repeatability standard deviation (or measurement error)
ρ	=	density of water
θ_w	=	Volumetric moisture content, bf, cf, and hr = SWCC curve fitting parameters
ψ	=	Matric suction

ψ_r = SWCC curve fitting parameter

REFERENCES

1. B.R. Christopher and V. C. McGuffey. *Pavement Subsurface Drainage Systems*, Synthesis of Highway Practice 239, National Cooperative Highway Research Program, Transportation Research Board, National Academy Press, Washington, D.C., 1997.
2. H.R. Cedergren. America's Pavement: World's Longest Bathtubs. Civil Engineering, Vol. 64, Series 9, 1994, pp. 56–58.
3. *AASHTO Design Guide for Design of Pavement Structures*. American Association of State Highway and Transportation Officials, Washington D.C., 1993.
4. NCHRP 1-37A. *Guide for Mechanistic-Empirical Design of New and Rehabilitated Pavement Structures*. Final Report NCHRP 1-37A, National Cooperative Highway Research Program, Transportation Research board, Washington, D.C., 2004.
5. L.K. Moulton. *Highway Subdrainage Design.* Report No. FHWA-TS-80-224. Federal Highway Administration, Washington, D.C., 1980.
6. D. R. Nielsen, J.W. Biggar, and H.T. Erh. Spatial Variability of Field-Measured Soil-Water Properties. Hilgardia, Vol. 42, 1973, pp. 215-260.
7. A.W. Warrick. *Soil Physics Companion*. CRC Press, Boca Raton, Florida, 2002.
8. D.J. White, P. Vennapusa, and C.T. Jahren. *Determination of the Optimum Base Characteristics for Pavements*. Final Report, Iowa DOT Project TR–482, Centre of Transportation Research and Education Project 02-119, Iowa State University, Ames, Iowa, 2004.
9. D. Kirkham. Field Method for Determination of Air Permeability of Soil in its Undisturbed State. Soil Science Society of America Proceedings, Vol. 11, 1946, pp. 93–99.
10. B.L. Grover. Simplified Air Permeameters for Soil In Place. Soil Science Society of America Proceedings, Vol. 19, 1955, pp. 414–418.
11. E.C. Steinbrenner. A Portable Air Permeameter for Forest Soils. Soil Science Society of America Proceedings, Vol. 23, 1959, pp. 478–481.
12. B.V. Iverson, P. Schjønning, T.G. Poulsen, and P. Moldrup. In situ, On-Site and Laboratory measurements of Air Permeability: Boundary Conditions and Measurement Scale. Soil Science Society of America Proceedings, Vol. 166, 2001, pp. 97–106.
13. M. Jalbert and J.H. Dane. A Handheld Device for Intrusive and Nonintrusive Field Measurements of Air Permeability. Vadose Zone Journal, Vol. 2, 2003, pp. 611–617.
14. J.M. Davis, J.L. Wilson, and F.M. Phillips. A Portable Air-Minipermeameter for Rapid In Situ Field Measurements. Ground Water, Vol. 32, 1994, pp. 258–266.
15. R. Eijpe and K.J.Weber. Mini-permeameters for consolidated rock and unconsolidated sand. American Association of Petroleum Geology, Bulletin 55, 1971, 307–309.
16. J.D. Goggin, L.R. Thrasher, and W.L. Lake. A Theoretical and Experimental Analysis of Minipermeameter Response Including Gas Slippage and High Velocity Flow Effects. In situ, Vol. 12, 1988, pp. 79-116.
17. K. Chief, T.P.A. Ferré, and B. Nijssen. Field testing of a soil corer air permeameter (SCAP) in desert soils. Vadose Zone Journal, Vol. 5, 2006, 1257–1263.
18. A. Amoozegar and A.W. Warrick. Hydraulic Conductivity of Saturated Soils – Field Methods. In Methods of Soil Analysis, Part 1: Physical and Mineralogical methods, Agronomy Monograph 9, American Society of Agronomy, Madison, WI, 1986.
19. H. Bouwer. Intake Rate: Cylinder Infiltrometer. In Methods of Soil Analysis Part 1: Physical and Mineralogical Methods, Agronomy Monograph 9, American Society of Agronomy, Madison, WI, 1986.
20. ASTM D3385-03. *Standard Test Method for Infiltration Rate of Soils in Field Using Double-Ring Infiltrometer*. ASTM International, West Conshohocken, PA, 2009.
21. H. Bouwer. Measuring Horizontal and Vertical Hydraulic Conductivity of Soil with the Double-Tube Method. Soil Science Society of America Proceedings, Vol. 28, 1964, pp. 19–23.
22. D. Reynolds and D.E. Elrick. A Method for Simultaneous In-Situ Measurement in the Vadose Zone of Field Saturated Hydraulic Conductivity, Sorptivity, and the Conductivity-Pressure Head Relationship. Ground-Water Monitoring Review, Vol. 6, No. 4, 1986.
23. Y. Mualem. A New Model for Predicting the Hydraulic Conductivity of Unsaturated Porous Media. Water Resources Research, Vol. 12, 1976, pp. 513–522.

24. T. Wells, S. Fityus, D.W. Smith, and H. Moe. The Indirect Estimation of Saturated Hydraulic Conductivity of Soils, Using Measurements of Gas Permeability. I. Laboratory Testing with Dry Granular Soils. Australian Journal of Soil Research, 44, 2006, pp. 719–725.

25. D.L. Allen, D.B. Schultz, and L.J. Fleckenstein. *Development and Proposed Implementation of a Field Permeability Test for Asphalt Concrete.* Research Report KTC-01-19/SPR216-00-1F, Kentucky Transportation Center, University of Kentucky, Kentucky, 2001.
26. J.M. Roberts. *Void and Texture Parameters Affecting Asphaltic Pavement Skid Resistance.* Master's Thesis, Department of Civil Engineering, Pennsylvania State University, Pennsylvania, 1970.
27. D.L. Standiford, R.A. Graul, and L.R. Lenke. *Permeability Equipment for Porous Friction Surface*. Interim Report DOT/FAA/PM-85/31, U.S. Department of Transportation, Washington, D.C, 1985.
28. G. Lees and I.E.D. Katekhda. Prediction of Medium and High Speed Skid Resistance Values by Means of a Newly Developed Outflow Meter. Proceedings –Association of Asphalt Paving Technologists, Vol. 43, 1974, pp. 436–464.
29. W.H. Gotolski, R.W. Smith, and J.M. Roberts. *Permeance as a Mix Design Criterion for Asphaltic Concrete Pavements*. Pennsylvania Department of Highways Research Project No. 68-1, Department of Civil Engineering, Pennsylvania State University, Pennsylvania, 1970.
30. L.K. Moulton and K.R. Seals. *Determination of the In-situ permeability of Base and Subbase courses.* Final Report No. FHWA-RD-79-88, Department of Civil Engineering, West Virginia University, West Virginia, 1979.
31. T.R. Clyne, V.R. Voller, and B. Birgisson, B. *Evaluation of Field Permeameter to Measure Saturated Hydraulic Conductivity of Base/Subgrade Materials*, Report No. Mn/RC – 2001-19, Minnesota Department of Transportation, St. Paul, Minnesota, 2001.
32. D.J. White, P. Vennapusa, M.T. Suleiman, C.T. Jahren. An In-situ Device for Rapid Determination of Permeability for Granular Bases. Geotechnical Testing Journal, Vol. 30, No. 4, 2007, pp. 282–291.
33. P. Vennapusa, D.J. White, C.T. Jahren. In-Situ Permeability of Unbound Granular Bases Using the Air Permeameter Test. Proceedings of 85th Transportation Research Board Annual Meeting, Washington, D.C., January 2006.
34. Lenox Laser. *Fluid Flow Through Small Calibrated Orifices.* Lenox Laser, Glen Arm, Maryland <http://www.lenoxlaser.com/flowproducts/pdf/fluid_flow_through_calibrated_orifices.pdf> (Accessed 10/24/2009).
35. R.H. Brooks and A.T. Corey. Hydraulic Properties of Porous Media. Hydrology Papers, No. 3, Colorado State University, Fort Collins, Colorado, 1964.
36. J. Côté and J.M. Konrad. Assessment of the Hydraulic Characteristics of Unsaturated Base-Course Materials: A Practical Method for Pavement Engineers. Canadian Geotechnical Journal, Vol. 40, 2003, pp. 121–136.
37. S.M. Levorson. *Mechanics of Unsaturated Granular Media*, Doctoral Thesis, Department of Civil Engineering, Iowa State University, Ames, Iowa, 1993.
38. C.E. Zapata and W.N. Houston. *Calibration and Validation of the Enhanced Integrated Climatic Model for Pavement Design.* NCHRP Report 602, Transportation Research Board, Washington, D.C., 2008.
39. D.G. Fredlund and A. Xing (1994). Equations for the Soil-Water Characteristic Curve. Canadian Geotechnical Journal, Vol. 31, No. 4, 1994, pp. 521–532.
40. D.P. Cudoto. *Foundation Design Principles and Practices.* 2nd Edition, Prentice-Hall, Englewood Cliffs, New Jersey, 1999.
41. ACPA. *Drainage in Concrete Pavement Structures.* Concrete Pavement Technology Series, American Concrete Pavement Association, Skokie, Illinois, 2008.
42. J.W. Hall, J. Mallela, and K.L. Smith. *Stabilized and Drainable Base for Rigid Pavement: A Design and Construction Guide*. Innovative Pavement Research Foundation Report IPRF-01-G-002-021(G), Applied Research Associates, Skokie, Illinois, October 2005.
43. G.E. Laliberte, A.T. Corey, and R.H. Brooks. Properties of Unsaturated Porous Media. Hydrology Papers, No. 17, Colorado State University, Fort Collins, Colorado, 1966.
44. S.F. Averjanov. About Permeability of Subsurface Soils in Case of Incomplete Saturation," Engineering Collection, Vol. 7, as Quoted by P. Ya Palubarinova, 1962. The Theory of Ground Water Movement (English Translation by I. M. Roger DeWiest. Princeton University Press, Princeton, NJ), pp. 19–21. 1950.
45. H.R. Cedergren, J.R. Arman, and K.H. O'Brien. *Development of Guidelines for the design of Subsurface Drainage Systems for Highway Structural Systems.* Final Report, Federal Highway Administration, Washington, D.C., February 1973.
46. D.J. White, M. Thompson, P. Vennapusa. *Field Validation of Intelligent Compaction Monitoring Technology for Unbound Materials.* Minnesota Department of Transportation Final Report No. MN/RC-2007-10, St. Paul, Minnesota, April 2007.

47. D.J. White, P. Vennapusa, H. Gieselman, L. Johanson, R. Goldsmith. ***Accelerated Implementation of Intelligent Compaction Monitoring Technology for Embankment Subgrade Soils, Aggregate Base, and Asphalt Pavement Materials*** TPF-5(128) **– *Texas IC Demonstration Field Project***, Report submitted to The Transtec Group, FHWA, November 2008.
48. D.J. White, P. Vennapusa, H. Gieselman, J. Zhang, R. Goldsmith, L. Johanson, S. Quist. ***Accelerated Implementation of Intelligent Compaction Monitoring Technology for Embankment Subgrade Soils, Aggregate Base, and Asphalt Pavement Materials*** TPF-5(128) **– *Texas NY Demonstration Field Project***, Preliminary Data Report submitted to The Transtec Group, FHWA, June 2009.
49. E.H. Isaaks and R.M. Srivastava. *An Introduction to Applied Geostatistics*. Oxford University Press, New York, 1989.
50. I. Clark and W. Harper. *Practical geostatistics 2000*. 3rd reprint, Ecosse North America Llc, Columbus, Ohio, 2002.
51. D.G. Krige. *A statistical approach to some mine valuations and allied problems at the Witwatersrand*. M.S. Thesis, University of Witwatersrand, Johannesburg, South Africa, 1951.

APPENDIX

APPENDIX A: CROSS-SECTIONAL DRAWINGS OF APT COMPONENTS

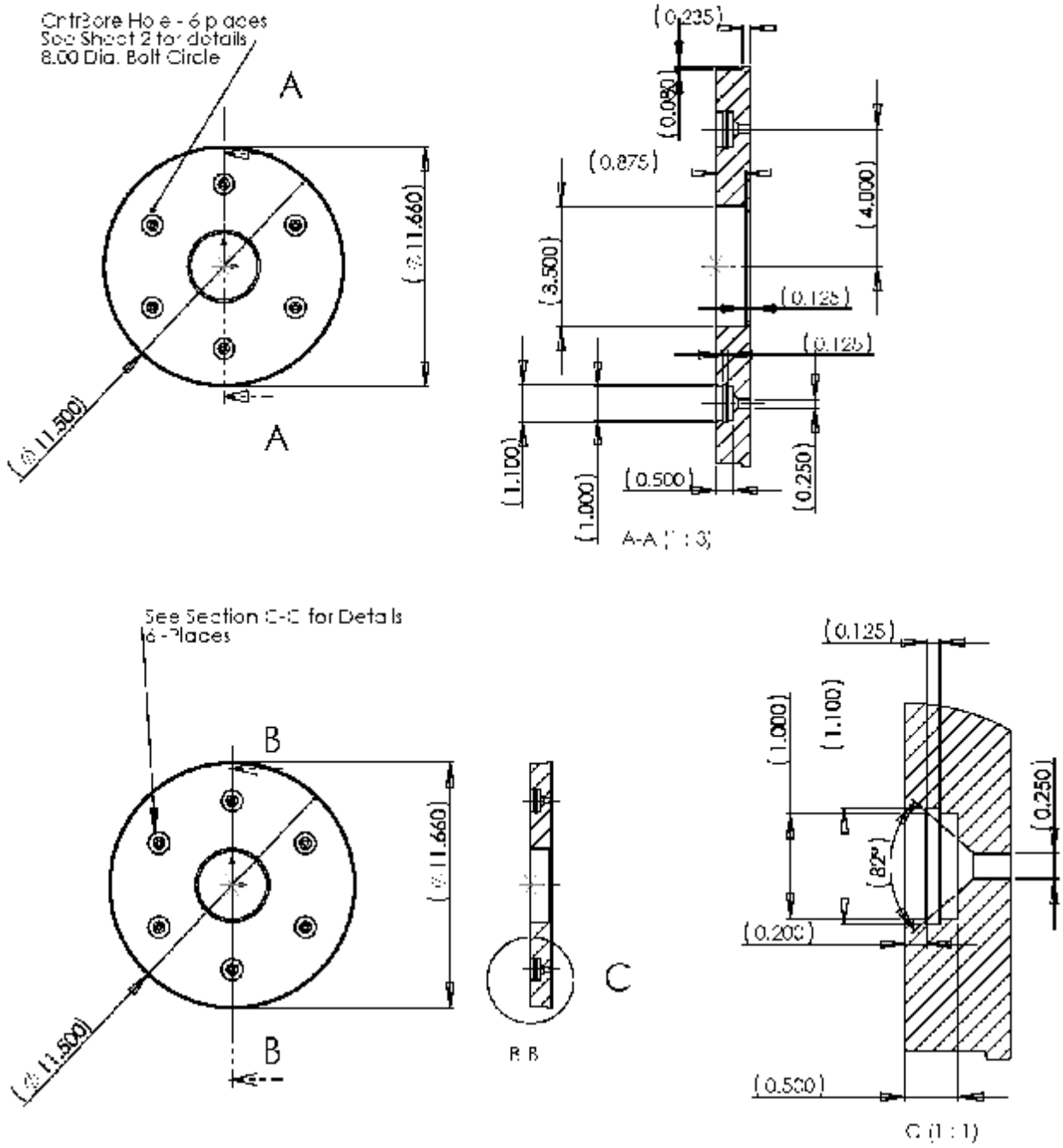

APPENDIX B: FLOW RATE CALCULATION AND THEORETICAL MODEL

Flow rate is calculated using the following equation:

$$Q = 0.01749 \times \frac{P_i}{29.7} \times \sqrt{\frac{29}{M}} \times CF \times \sqrt{\frac{528}{T}} \times d^2$$

where: Q = volumetric flow rate (cm^3/min); P_i = absolute pressure at the orifice inlet (psi); M = molecular weight of gas (Air = 29, Nitrogen = 28, CO_2 = 44); T = temperature (Rankine); CF = correction factor based on $\Delta P/P_i$; $\Delta P = P_i - P_o$; P_o = absolute pressure at the orifice outlet (psi); d = orifice diameter (micrometer).

CF is obtained from the following table:

$\Delta P / P_i$	CF
0.52	1
0.48	0.994
0.44	0.983
0.4	0.966
0.36	0.944
0.32	0.918
0.28	0.884
0.24	0.845
0.2	0.782
0.16	0.715
0.12	0.638
0.08	0.542
0.04	0.382

To simplify the program code in the output meter, a three-parameter hyperbolic model is fit to the pressure-flow model to estimate the flow rate, Q. The hyperbolic model used is as follows:

$$Q(cfh) = \frac{a \times Pressure}{b + Pressure} + c \times Pressure$$

The pressure in the above equation is the gauge pressure. The model parameters a, b, c for APT (A), (B), (C), and (D) models are presented in the following figure.

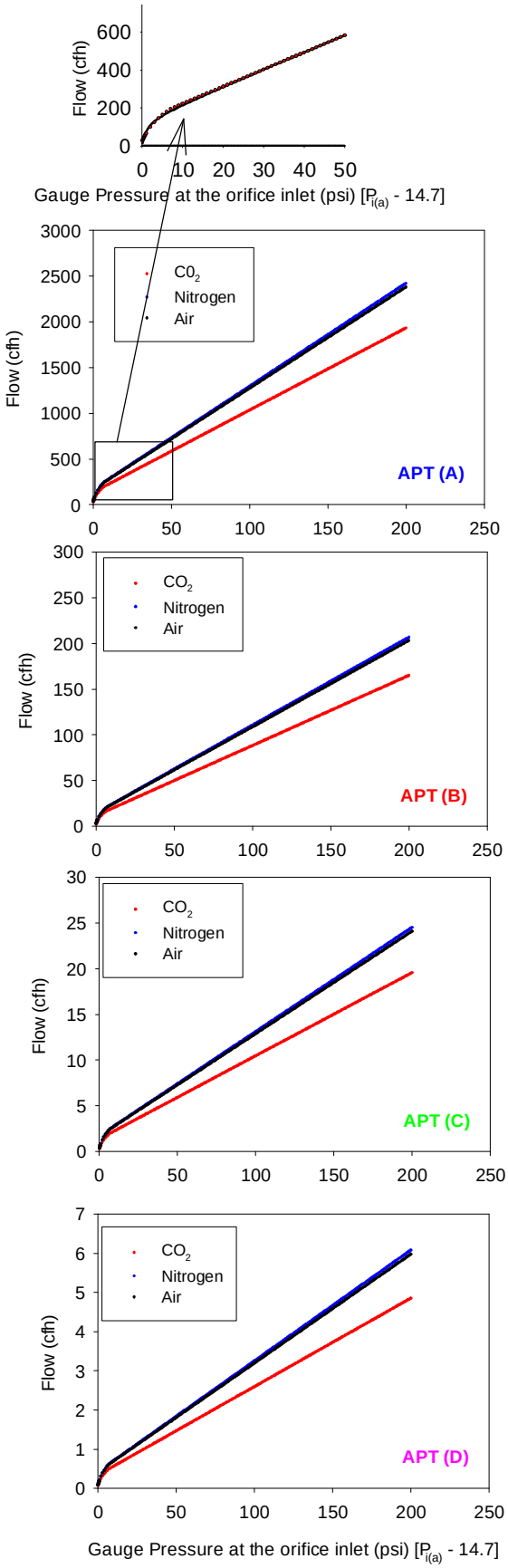

APT Flow-Pressure Model Parameters

Model: Flow (cfh) =a*x/(b+x)+c*x

where "x" is the inlet pressure in psi

APT (A) Model with 2982 micron orifice			
Regression Coefficients	**Air**	**Nitrogen**	**CO_2**
a	170.4730	173.4905	138.3975
b	1.1044	1.1044	1.1044
c	11.0346	11.2299	8.9584
R^2	1.0000	1.0000	1.0000
Standard Error	3.4481	3.5091	2.7993

APT (B) Model with 870.95 micron orifice			
Regression Coefficients	**Air**	**Nitrogen**	**CO_2**
a	14.5421	14.7995	11.8059
b	1.1044	1.1044	1.1044
c	0.9413	0.9580	0.7642
R^2	1.0000	1.0000	1.0000
Standard Error	0.2941	0.2993	0.2388

APT (C) Model with 293.66 micron orifice			
Regression Coefficients	**Air**	**Nitrogen**	**CO_2**
a	1.7254	1.7559	1.4007
b	1.1044	1.1044	1.1044
c	0.1117	0.1137	0.0907
R^2	1.0000	1.0000	1.0000
Standard Error	0.0349	0.0355	0.0283

APT (C) Model with 149.41 micron orifice			
Regression Coefficients	**Air**	**Nitrogen**	**CO_2**
a	0.4280	0.4355	0.3474
b	1.1044	1.1044	1.1044
c	0.0277	0.0282	0.0225
R^2	1.0000	1.0000	1.0000
Standard Error	0.0087	0.0088	0.0070

Otek Output Meter Program Code

Program for 2982 micrometer Orifice APT (A) Based on Hyperbolic Equation

APPROXIMATE MAXIMUM Q = 2000 cfh using Air (change regression coefficients to shown in Figure above for CO_2 and Nitrogen)

```
S01 DFIX11
S01 DFIX22
S01 DFIX32
S01 CH1ON
S01 CH2ON
S01 CH3ON
S01 EQN1 S1=C1
S01 EQN2 S2=C2
S01 EQN3 S3=(170.4730*C1)
S01 EQN4 S4=(1.1044+C1)
S01 EQN5 S5=(11.0346*C1)
S01 EQN6 S6=(S3/S4)+(S5)
S01 EQN7 S7=1
S01 STREAM1 +DISP1
S01 STREAM2 +DISP2
S01 STREAM6 +DISP3
S01 SCALE1 15.625
S01 SCALE2 0.1875
S01 SCALE3 15.625
S01 OFFSET1 -62.5
S01 OFFSET2 -0.75
S01 OFFSET3 -62.5
S01 RUN
S01 WRITE
```

Program for 870.95 micrometer Orifice APT (B) Based on Hyperbolic Equation

APPROXIMATE MAXIMUM Q = 200 cfh using Air (change regression coefficients to shown in Figure above for CO_2 and Nitrogen)

```
S01 DFIX11
S01 DFIX22
S01 DFIX32
S01 CH1ON
S01 CH2ON
S01 CH3ON
S01 EQN1 S1=C1
S01 EQN2 S2=C2
S01 EQN3 S3=(14.5421*C1)
S01 EQN4 S4=(1.1044+C1)
S01 EQN5 S5=(0.9413*C1)
S01 EQN6 S6=(S3/S4)+(S5)
```

S01 EQN7 S7=1
S01 STREAM1 +DISP1
S01 STREAM2 +DISP2
S01 STREAM6 +DISP3
S01 SCALE1 15.625
S01 SCALE2 0.1875
S01 SCALE3 15.625
S01 OFFSET1 -62.5
S01 OFFSET2 -0.75
S01 OFFSET3 -62.5
S01 RUN
S01 WRITE

Program for 293.66 micrometer Orifice APT(C) Based on Hyperbolic Equation

APPROXIMATE MAXIMUM Q = 20 cfh using Air (change regression coefficients to shown in Figure above for CO_2 and Nitrogen)
S01 DFIX11
S01 DFIX22
S01 DFIX32
S01 CH1ON
S01 CH2ON
S01 CH3ON
S01 EQN1 S1=C1
S01 EQN2 S2=C2
S01 EQN3 S3=(1.7254*C1)
S01 EQN4 S4=(1.1044+C1)
S01 EQN5 S5=(0.1117*C1)
S01 EQN6 S6=(S3/S4)+(S5)
S01 EQN7 S7=1
S01 STREAM1 +DISP1
S01 STREAM2 +DISP2
S01 STREAM6 +DISP3
S01 SCALE1 15.625
S01 SCALE2 0.1875
S01 SCALE3 15.625
S01 OFFSET1 -62.5
S01 OFFSET2 -0.75
S01 OFFSET3 -62.5
S01 RUN
S01 WRITE

Program for 149.41 micrometer Orifice APT(D) Based on Hyperbolic Equation

APPROXIMATE MAXIMUM Q = 5 cfh using Air (change regression coefficients to shown in Figure above for CO_2 and Nitrogen)
S01 DFIX11
S01 DFIX22

```
S01 DFIX32
S01 CH1ON
S01 CH2ON
S01 CH3ON
S01 EQN1 S1=C1
S01 EQN2 S2=C2
S01 EQN3 S3=(0.4280*C1)
S01 EQN4 S4=(1.1044+C1)
S01 EQN5 S5=(0.0277*C1)
S01 EQN6 S6=(S3/S4)+(S5)
S01 EQN7 S7=1
S01 STREAM1 +DISP1
S01 STREAM2 +DISP2
S01 STREAM6 +DISP3
S01 SCALE1 15.625
S01 SCALE2 0.1875
S01 SCALE3 15.625
S01 OFFSET1 -62.5
S01 OFFSET2 -0.75
S01 OFFSET3 -62.5
S01 RUN
S01 WRITE
```

APPENDIX C: GPT TEST PROCEDURE

METHOD OF TEST
IN-SITU GAS PERMEAMETER TEST FOR PAVEMENT BASE AND SUBBASE MATERIALS

SCOPE

This test method describes the procedure for determining the in-situ saturated hydraulic conductivity of pavement base/subbase materials using the gas permeameter test [GPT] device. Measurements are limited to materials with hydraulic conductivity between 10^{-4} to 10 cm/s.

DEFINITION

Gas Permeability – It is defined as a factor of proportionality between the rate of gas flow and the pressure gradient along the flow distance.

Saturated Hydraulic Conductivity – It is defined as the rate of discharge of water at 20°C under conditions of laminar flow through a unit cross-sectional area of a soil medium under a unit hydraulic gradient.

APPARATUS

The GPT device is shown in Figure 1. The GPT unit is self-contained with two compressed gas cylinders attached to the wheel cart. With two carbon dioxide (CO_2) cylinders, more than 50 tests can be performed before refilling the cylinders. The unit can be mounted on to a wheel cart on large rubber wheels to allow for easy transporting and handling in the field. The gas flow is controlled using a regulator and a replaceable precision orifice located inside the ruggedized housing. The gauge pressure at the inlet and the outlet of the orifice are monitored using digital pressure transducers to calculate flow rate. The use of precision orifice to calculate flow rate allows for high precision even at low pressures (i.e., < 1 in of water pressure). The inlet pressure transducer is of 0 to 250 psi range and the outlet pressure transducer is of 0 to 3 in of water [H_20] range. The inlet and outlet gauge pressures and calculated flow rate measurements are displayed on a programmable digital display panel attached to the top cover plate. The digital display panel is connected to a rechargeable battery mounted inside the ruggedized housing. Data obtained during the test can be transferred to a computer via the RS-232 port and the auxiliary switch on the top cover plate. The base plate is fabricated using an abrasive resistant polymer and is replaceable if needed. A polyurethane base seal is attached to the base plate. The test is performed by placing the GPT unit on closed-cell compressible foam to effectively seal the base and prevent gas leakage.

Figure 1. Gas Permeameter Test (GPT) Device

EQUIPMENT

A. GPT Unit
B. Compressed air or CO_2 or nitrogen tank and regulator,
C. ½ in. hose with quick connections at both ends,
D. A wrench to fix the regulator to the compressed air tank,
E. 1 in. thick closed cell compressible foam of 11.5 in. diameter with a 3.5 in. diameter hole in the center.

TEST PROCEDURE

There are several steps required to use the GPT effectively in the field but first, the basic information for using the GPT is listed below (Quick Startup and use of the GPT). Following that will be a more detailed description of the programming details for the device.

The APT device is usually attached to a two-wheeled cart that allows it to be moved quickly into position and lowered onto the surface. Once lowered onto the surface, a "free-float" mechanism on the cart insures the GPT is sitting firmly on the subbase material, kept in place by its own weight. The two-wheeled cart also carries a pair of 20-pound CO_2 cylinders of gas. A step down regulator feeds gas to the GPT faceplate via a flexible hose and quick-connect coupler.

Quick Setup and use of the GPT in the field:

- Assemble the GPT two-wheeled cart; attach CO_2 cylinders and the regulator with the flexible "quick-connect" hose.
- Remove the GPT device from the carrying case and place on the "free-float" pins.
- Attach the CO_2 hose using the "quick-connect" fitting
- Open the CO_2 cylinder valve
- Roll the cart and GPT device to the appropriate location and lower the GPT on the subbase surface (note- the surface is smoothed reasonably flat prior to placement) and make sure it is "free floating" from the cart.

1. Turn on the GPT device, allow for warm-up and start the measuring procedure as follows:
2. Read and record the values for P1, P2 and Flow at a "Zero" P1 level. Note that the P1 and P2 values displayed on the device are $P_{i(g)}$ and $P_{o(g)}$, respectively in the calculations.
3. Turn the Pressure/Flow regulator knob to raise the P1 value and take readings at various points – allow the P1 pressure to stabilize prior to recording P2 or Vol.

General Data Collection Procedure:

The GPT is currently set up to collect and store the data using the following procedure.

1. Connect the APT to a computer using HyperTerminal (a standard Windows program)

2. Test the connection by turning on the GPT while the serial cable is connected and the following message will appear on the screen

   HI-Q by OTEK
   Ver. 3.03
   Address: '01'
   Warming up...done
   *****

Data Collection Procedure:

1. Start up HyperTerminal (using the PUFF2 program to connect)

2. Go to the TRANSFER option on the Menu (Upper portion of the screen)

3. Select Capture Text

4. A “Capture Text” box will open

5. Name the file and provide a location

6. Select START

7. The box will close and the system is ready to start collecting data

8. Press the MENU button on the meter panel face to Reset the Counter/Timer to Zero and collect the 1st data set

9. Turn up the regulator as required

10. Press the ENTER button to collect the 2nd set of data and all subsequent data at a particular location.

11. When done collecting data at a particular location, there are 2 options to consider for additional locations.

    Option #1 – saving each data set in a separate File

    At this point you can either STOP the data collection by going to the Menu/ Capture Text and choosing STOP. This will stop the data collection process and save the data file to your original file name.

    Option #2 – saving data continuously in a single file with the data separated by a ZERO in the Time Line

    Go to the next test point

    Press the MENU button the meter panel (this generates the 1st data set for that location and places a ZERO in the TIME Line location (use this to help separate data sets)

    Press the ENTER button to collect the 2nd set of data and all subsequent data at a particular location.

    Collect data – make notes on what you have done to keep track.

HIQ-126 OTEK Digital Meter Setup and Programming Notes:

The HIQ-126 OTEK Digital Meter is programmable using Hyper Terminal software. The device will need to be programmed whenever the orifice diameter, type of gas (e.g., Air, CO_2, or Nitrogen), units of measure or decimal point location is changed. In some cases the program may need to be reloaded if the battery is allowed to run too low on power. If the digital meter display starts blinking, it may be a sign of low battery voltage. Shut the unit OFF and plug in the AC charger. Check to see if the program and sub-routines are still in place before additional use. It will require reprogramming if the internal algorithms are modified. Internal algorithms determine how input data is manipulated or used for other inputs.

Programming the HIQ-126 (OTEK Digital Meter) requires a computer for communication with the digital meter via the Hyper Terminal program (which is a standard Microsoft Windows interface program). Communication is handled via a panel mounted RS-232 interface plug (DB-9 connector) on the device faceplate. In addition, the following programs or hardware will be needed or useful:

- Text Editor - Note Pad, TextPad or Word – used to write new programs, review or edit data
- HIQ-126 (OTEK Digital Meter OTEK) manual. Refer to the HIQ-126 manual for details.
- Excel spreadsheet program - an effective way to analyze and graph data.
- Laptop computer - used for collection of field data.

The HIQ –126 meter uses 3 digital meters to display the information from the GPT.

- Display # 1 – Top - displays the Input value of Pressure P1 – PSIG ($P_{i(g)}$ in the calculations)
- Display # 2 – Middle - displays the Chamber Back Pressure P2 Inches of Water ($P_{o(g)}$ in the calculations)

- Display # 3 – Bottom - displays the Flow Rate of the test gas Cubic Feet/Hour – Calculated (Q in the calculations)

The program codes developed for GPT (A)(B)(C)(D) and air, nitrogen, and CO_2 gases are provided in Appendix B. These codes are transferred to the HIQ-126 OTEK Digital Meter using the Hyper Terminal program. The steps involved in the programming are as follows:

1. Save the appropriate program codes provided in Appendix B as a *.txt file
2. Start the HyperTerminal (using the PUFF2 program to connect)
3. Go to the TRANSFER option on the Menu (Upper portion of the screen)
4. Select Send Text File and select the text file saved as part of Step 1

The program code will appear in the hyper terminal program. After the programming is finished, the GPT device is ready for measurements.

CALCULATIONS

A. Determine the Geometric Factor (G_o) based on the estimated thickness of the aggregate layer (L) at the test location using Figure 2.

B. Use the range of saturation values provided in Table 1 to estimate S for the calculations. For better accuracy, determine the in-situ dry density and moisture contents at each test location and calculate S using equation A.

$$S = \frac{G_s w}{\left(\frac{G_s \gamma_w}{\gamma_d} - 1\right)} \qquad [A]$$

Where:

S = Degree of saturation
G_s = Specific gravity (Assume 2.70 if unknown)
w = Moisture content
γ_w = Unit weight of water (62.4 pcf)
γ_d = Dry unit weight of the material (pcf)

C. Calculate the saturated hydraulic conductivity K_{sat} (cm/sec) using equation B:

$$K_{sat} = \left[\frac{2\mu_{gas} Q P_1}{r G_o \left(P_1^{\,2} - P_2^{\,2}\right)}\right] \times \frac{\rho g}{\mu_{water}\left(1 - S_e\right)^2 \left(1 - S_e^{((2+\lambda)/\lambda)}\right)} \qquad [B]$$

where:

K_{sat} = Saturated hydraulic conductivity (cm/sec)
μ_{gas} = Kinematic viscosity of the gas (Pas) (CO_2: 1.48E-05, Air: 1.83E-05, Nitrogen: 1.78E-05)
P_1 = Absolute gas pressure on the soil surface (Pa) = $P_{o(g)}$ * 250 + 101325
$P_{o(g)}$ = Gauge pressure at the orifice outlet (inches of H_20)
P_2 = Atmospheric pressure (Pa) = 101325
Q = flow rate (cm^3/s)
r = radius at the outlet (cm) = 4.45
G_0 = Geometric factor determined from Figure 2
μ_{water} = Absolute viscosity of water (g/cm-s) = 0.01
ρ = Density of water (g/cc) = 1
g = Acceleration due to gravity (cm/s^2) = 981
S_e = Effective saturation [$S_e = (S - S_r)/(1-S_r)$]
S = Field saturation (from step B)
S_r = Residual saturation (determine based on soil type from Table 2)

λ = Brooks-Corey pore size distribution index (determine based on soil type from Table 2)

A sample calculation sheet and an example calculation are provided below.

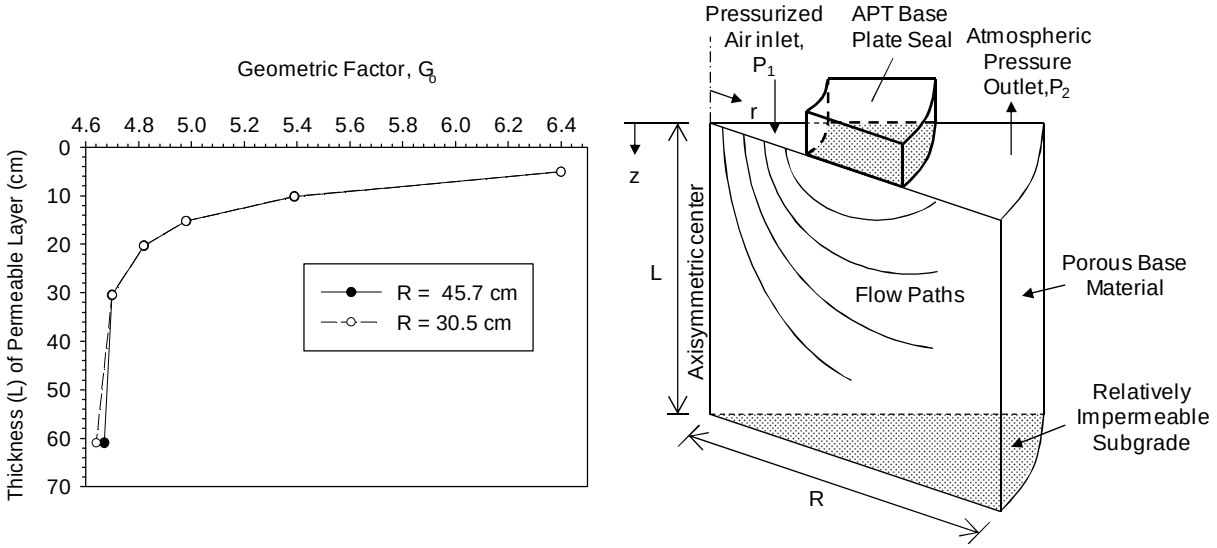

Figure 2. Graph to determine Geometric factor G_o for GPT Device

TABLE 1 Summary of typical field saturation values reported in the literature for granular base/subbase materials

		Field Saturation, S (%)[†]	
Material Type	Classification (USCS, AASHTO)	Mean	COV (%)
Crushed Lime Stone	GP-GM, A-1-a	16	20
Reclaimed Asphalt	GP-GM, A-1-a	28	49
Crushed Recycled Concrete	GW-GM, A-1-a	45	9
Crushed Lime Stone	GP-GC, A-1-a	19	17
Crushed Recycled Concrete	GP, A-1-a	37	19
Crushed Gravel	SP-SM, A-1-b	53	9
Crushed Gravel	SP-SM, A-1-b	44	31
Flex Base Material	GP-GM, A-1-a	58	15
Crushed Sandstone	GW	62	9
Crushed Limestone	GP-GM, A-1-a	36	19
Crushed Slag	GP-GM, A-1-a	24	24
Cement Treated Base	GP, A-1-a	35	15

[†]field saturation values determined from in-situ moisture and density measurements using a nuclear gauge.

TABLE 2 Summary of residual saturation and pore size distribution index values reported in the literature and typical values calculated using equations 6 to 18 for granular materials

Material Type or USCS Classification	Residual Saturation (S_r)	Pore Size Distribution Index, λ
Touchet Silt Loam[1]	18 to 22	1.02 to 1.70
Columbia Sandy Loam[1]	18 to 22	1.27 to 1.70
Unconsolidated Sand[1]	8 to 9	4.02 to 4.75
Volcanic sand[2]	16	2.29
Fine sand[2]	17	3.7
Glass beads[2]	9	7.3
Natural Sand Deposits[2]	—	4
Crushed Granite[2]	—	0.33 to 0.36
Crushed Shale[2]	—	0.23 to 0.27
Crushed Limestone[2]	—	0.22 to 0.31
Range of values for typical filter materials and open graded bases (5)		
SW (Filter Materials)	10 to 11	0.65 to 2.15
SP (Filter Materials)	10	11.15
GP (Open Graded Bases)	1 to 2	17.26 to 18.20
Range of values determined for granular materials used in this study		
SP	10	2.20 to 4.08
SW-SM	11	0.54
GP	2 to 5	3.65 to 4.62
GP-GM	11 to 15	0.59 to 0.98

(1) G.E. Laliberte, A.T. Corey, and R.H. Brooks. Properties of Unsaturated Porous Media. Hydrology Papers, No. 17, Colorado State University, Fort Collins, Colorado, 1966.
(2) R.H. Brooks and A.T. Corey. Hydraulic Properties of Porous Media. Hydrology Papers, No. 3, Colorado State University, Fort Collins, Colorado, 1964.
(3) S.F. Averjanov. About Permeability of Subsurface Soils in Case of Incomplete Saturation," Engineering Collection, Vol. 7, as Quoted by P. Ya Palubarinova, 1962. The Theory of Ground Water Movement (English Translation by I. M. Roger DeWiest. Princeton University Press, Princeton, NJ), pp. 19–21. 1950.
(4) J. Côté and J.M. Konrad. Assessment of the Hydraulic Characteristics of Unsaturated Base-Course Materials: A Practical Method for Pavement Engineers. Canadian Geotechnical Journal, Vol. 40, 2003, pp. 121–136.
(5) H.R. Cedergren, J.R. Arman, and K.H. O'Brien *Development of Guidelines for the design of Subsurface Drainage Systems for Highway Structural Systems.* Final Report, Federal Highway Administration, Washington, D.C., February 1973.

SAMPLE DATA SHEET

Date: _____
Project ID: _____
Location: _____
Operator: _____
Material: _____

Initial Values:

Initial P1:	_____	PSIG	(1)
Initial P2:	_____	inches of H_20	(2)
Initial Q:	_____	CFH	(3)

GPT Readings:

Gas Used: _____

1st Reading				Corrected 1st Reading			
P1:	_____	PSIG	(4)	P1:	_____	PSIG	(7)=(4)-(1)
P2:	_____	inches of H_20	(5)	P2:	_____	inches of H_20	(8)=(5)-(2)
Q:	_____	CFH	(6)	Q:	_____	CFH	(9)=(6)-(3)
2nd Reading				Corrected 2nd Reading			
P1:	_____	PSIG	(10)	P1:	_____	PSIG	(13)=(10)-(1)
P2:	_____	inches of H_20	(11)	P2:	_____	inches of H_20	(14)=(11)-(2)
Q:	_____	CFH	(12)	Q:	_____	CFH	(15)=(12)-(3)
3rd Reading				Corrected 3rd Reading			
P1:	_____	PSIG	(16)	P1:	_____	PSIG	(19)=(16)-(1)
P2:	_____	inches of H_20	(17)	P2:	_____	inches of H_20	(20)=(17)-(2)
Q:	_____	CFH	(18)	Q:	_____	CFH	(21)=(18)-(3)
4th Reading				Corrected 4th Reading			
P1:	_____	PSIG	(22)	P1:	_____	PSIG	(25)=(22)-(1)
P2:	_____	inches of H_20	(23)	P2:	_____	inches of H_20	(26)=(23)-(2)
Q:	_____	CFH	(24)	Q:	_____	CFH	(27)=(24)-(3)

Develop P2 vs. Q relationship and determine Q at a desired P2 value.

[For example, P2 = 1 in of H_20]

P2:	_____	inches of H_20	(28)
Q:	_____	CFH	(29)

Density and Layer Thickness Measurements:

Dry Density, γ_d:	_____	pcf	(30)
Moisture, w:	_____	in decimals	(31)
Sp.Gr., G_s:	_____		(32) Assume 2.70 if unknown
Saturation, S:	_____		(33) =[(32)*(31)]/{[(32)*62.4/(30)]-1}
Thickness, L:	_____	cm	(34)

K_{sat} Calculation Parameters:

μ_{gas}:	_____	Pas	(35) (CO_2: 1.48E-05, Air: 1.83E-05, Nitrogen: 1.78E-05)
P_1:	_____	Pa	(36) =(28)*250+101325
P_2:	101325	Pa	(37)
Q:	_____	cm^3/s	(38) =(29)*7.86579
r:	4.45	cm	(39)
G_0:	_____		(40) Determine using Figure 2 based on (34)
r:	1	g/cc	(41)
μ_{water}:	0.01	g/cm-s	(42)
g:	981	cm/s^2	(43)
S_r:	_____		(44) Determine based on soil type from Table 3
S_e:	_____		(45) =[(33)-(44)]/[1-(44)]
λ:			(46) Determine based on soil type from Table 3

K_{sat} Calculation:

K_{sat}:	_____	cm/s	(47) $K_{sat} = \left[\frac{2\mu_{gas} Q P_1}{r G_o \left(P_1^2 - P_2^2\right)}\right] \times \frac{\rho g}{\mu_{water}\left(1-S_e\right)^2\left(1-S_e^{((2+\lambda)/\lambda)}\right)}$
K_{sat}:	_____	ft/day	(48) =(47)*2834.6

SAMPLE DATA SHEET— EXAMPLE CALCULATIONS

Date:	12/10/2009						
Project ID:	XYZ						
Location:	US69, Ames, Iowa						
Operator:	AB						
Material:	Well-Graded Sand						
Initial Values:							
Initial P1:	0.00	PSIG	(1)				
Initial P2:	0.00	inches of H_2O	(2)				
Initial Q:	0.00	CFH	(3)				
GPT Readings:							
Gas Used:	Air						
GPT orifice dia.	870.95	μm					
1st Reading				Corrected 1st Reading			
P1:	80.11	PSIG	(4)	P1:	80.11	PSIG	(7)=(4)-(1)
P2:	2.09	inches of H_2O	(5)	P2:	2.09	inches of H_2O	(8)=(5)-(2)
Q:	75.54	CFH	(6)	Q:	75.54	CFH	(9)=(6)-(3)
2nd Reading				Corrected 2nd Reading			
P1:	39.99	PSIG	(10)	P1:	39.99	PSIG	(13)=(10)-(1)
P2:	1.19	inches of H_2O	(11)	P2:	1.19	inches of H_2O	(14)=(11)-(2)
Q:	41.39	CFH	(12)	Q:	41.39	CFH	(15)=(12)-(3)
3rd Reading				Corrected 3rd Reading			
P1:	20.51	PSIG	(16)	P1:	20.51	PSIG	(19)=(16)-(1)
P2:	0.76	inches of H_2O	(17)	P2:	0.76	inches of H_2O	(20)=(17)-(2)
Q:	22.33	CFH	(18)	Q:	22.33	CFH	(21)=(18)-(3)
4th Reading				Corrected 4th Reading			
P1:	10.18	PSIG	(22)	P1:	10.18	PSIG	(25)=(22)-(1)
P2:	0.51	inches of H_2O	(23)	P2:	0.51	inches of H_2O	(26)=(23)-(2)
Q:	11.39	CFH	(24)	Q:	11.39	CFH	(27)=(24)-(3)
Develop P2 vs. Q relationship and determine Q at a desired P2 value.							
[For example, P2 = 1 in of H_2O]							
P2:	1.00	inches of H_2O	(28)				
Q:	32.10	CFH	(29)				
Density and Layer Thickness Measurements:							
Dry Density, γ_d:	108	pcf	(30)				
Moisture, w:	0.05	in decimals	(31)				
Sp.Gr., G_s:	2.7		(32)	Assume 2.70 if unknown			
Saturation, S:	0.24		(33)	=[(32)*(31)]/{[(32)*62.4/(30)]-1}			
Thickness, L:	15	cm	(34)				
K_{sat} Calculation Parameters:							
μ_{gas}:	1.83E-05	Pas	(35)	(CO_2: 1.48E-05, Air: 1.83E-05, Nitrogen: 1.78E-05)			
P_1:	101575	Pa	(36)	=(28)*250+101325			
P_2:	101325	Pa	(37)				
Q:	252.5	cm^3/s	(38)	=(29)*7.86579			
r:	4.45	cm	(39)				
G_0:	5		(40)	Determine using Figure 2 based on (34)			
r:	1	g/cc	(41)				
μ_{water}:	0.01	g/cm-s	(42)				
g:	981	cm/s^2	(43)				
S_r:	0.10		(44)	Determine based on soil type from Table 2			
S_e:	0.16		(45)	=[(33)-(44)]/[1-(44)]			
λ:	3		(46)	Determine based on soil type from Table 2			
K_{sat} Calculation:							
K_{sat}:	0.07	cm/s	(47)	$K_{sat} = \left[\frac{2\mu_{gas} Q P_1}{r G_o \left(P_1^2 - P_2^2\right)}\right] \times \frac{\rho g}{\mu_{water}\left(1-S_e\right)^2\left(1-S_e^{((2+\lambda)/\lambda)}\right)}$			
K_{sat}:	191.6	ft/day	(48)	=(47)*2834.6			

TRANSPORTATION RESEARCH BOARD 2009

EARTHWORKS ENGINEERING RESEARCH CENTER

Principal Investigators: David J. White, Ph.D., and Charles T. Jahren, Ph.D.
Research Associates: Pavana KR. Vennapusa, Ph.D. and Heath H. Gieselman

Self-Contained In-Situ Permeameter for Field QC/QA of Pavement Base/Subbase Materials – NCHRP-IDEA 130

Abstract
This project involves developing an automated rapid in-situ permeability test device for pavement base/subbase materials using an innovative gas-pressurized system. Rapid in-situ measurements can help better identify field problems such as segregation and particle degradation. State DOTs and contractors will be able to utilize the findings from this study as guidance for making informed decisions about how base/subbase construction specifications can be used to improve construction operations (e.g., spreading, trimming, etc.)

Project Tasks
Task 1: Build a new air permeameter test device
Task 2: Develop validation relationships with standard laboratory tests
Task 3: Perform field measurements at five different field projects
Task 4: Develop a database of soil-water retention characteristics of aggregate base
Task 5: Develop calibration guidelines

Description of the device
The air permeability test (APT) device (Fig. 1) consists of a self-contained console with internal ruggedized components, gas pressure regulator, precision orifice, and a circuit board for digital pressure readout. The console is connected to compressed CO_2 gas tanks. The contact base plate is specially fabricated and tested for effective sealing under different conditions. The whole unit is mounted on a wheel cart/pick-up system for easy transporting and handling in-situ.

Determination of *K* from APT
Using prescribed gas flow and pressure measurements from the device (Fig. 2) and the following equation derived based on expansion of the Darcy's law (see White et al. 2007[1]), the saturated hydraulic conductivity (K) can be determined.

$$K = \left[\frac{2\mu_{air} Q P_1}{a G_o (P_1^2 - P_2^2)}\right] \times \frac{\rho g}{\mu_{water}(1 - S_e)^2 (1 - S_e^{(12+\lambda)/\lambda})}$$

P_1 = chamber pressure ; P_2 = atmospheric pressure; Q = flow rate; G_o = geometric factor; S_e = effective saturation [$S_e = (S - S_r)/(1-S_r)$]; S = field saturation; S_r = residual saturation μ_{air} = kinematic viscosity of air; μ_{water} = absolute viscosity of water; a = chamber radius; ρ = density of water; g = gravity constant; and λ = pore size distribution index.

Laboratory and Field Studies
As a technique for validation, laboratory permeability tests were conducted on different materials. Comparison results are presented in Fig. 3. Ratio of mean K_{APT} and K_{LAB} range from 0.3 to 23.

To investigate spatial variation and the change in K in-situ as a function of percent fines (passing #200 sieve), a field study was conducted on a compacted pavement base layer on Hwy 63 in Iowa in a grid pattern (Fig. 4). Comparison of Kriged spatial maps of K from APT and percent fines show strong correlation (Figs. 4 and 5).

Product Pay-Off Potential
In-situ permeability measurements will allow greater precision in design, construction and field QC/QA. The use of this device presents a significant improvement in the state of practice for construction and field QC/QA of pavement base/subbase, which based on current trends of increasing subsurface drainage capacity in pavement design, should contribute to improving the service life of pavements.

Fig. 1. In-situ air permeameter test (APT)device

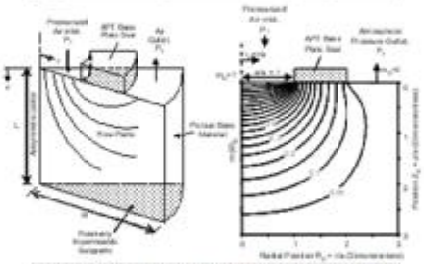

Fig. 2. Theoretical validation (White et al. 2007)[1]

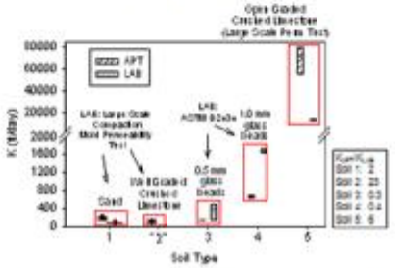

Fig. 3. Laboratory vs. field comparison test results

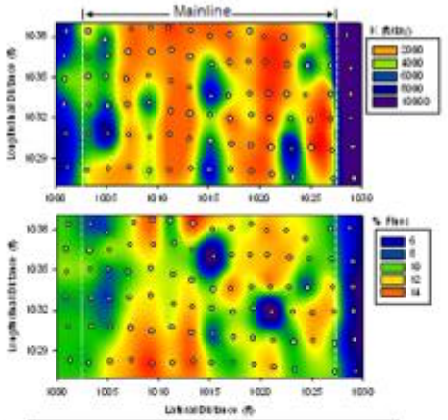

Fig. 4. Spatial comparison of *K* and % fines

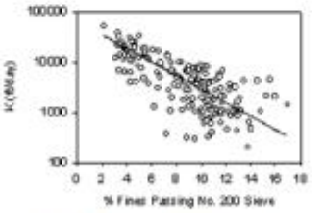

Fig. 5. Effect of % fines on in-situ *K*

Acknowledgements
NCHRP IDEA Highway Program, Eichner Engineering, EERC, Iowa DOT, and Handy Geotechnical Instruments, Inc.

[1] White, D., Vennapusa, P., Gieselman, H., Jahren, C. (2007). "An in-situ device for rapid determination of permeability for granular bases." Geotech. Test. J., 30(4), 282-291.